JOURNAL OF VIROLOGY, Aug. 2007, p. 7985–7992 Vol. 81, No. 15
0022-538X/07/$08.00+0 doi:10.1128/JVI.00429-07

Minimal Region Sufficient for Genome Dimerization in the Human Immunodeficiency Virus Type 1 Virion and Its Potential Roles in the Early Stages of Viral Replication[▽]

Jun-ichi Sakuragi,* Sayuri Sakuragi, and Tatsuo Shioda

Department of Viral Infections, Research Institute for Microbial Diseases, Osaka University, Osaka, Japan

Received 28 February 2007/Accepted 11 May 2007

It has been suggested that the dimer initiation site/dimer linkage sequence (DIS/DLS) region of the human immunodeficiency virus type 1 (HIV-1) RNA genome plays an important role at various stages of the viral life cycle. Recently we found that the duplication of the DIS/DLS region on viral RNA caused the production of partially monomeric RNAs in virions, indicating that this region indeed mediates RNA-RNA interaction. In this report, we followed up on this finding to identify the necessary and sufficient region for RNA dimerization in the virion of HIV-1. The region thus identified was 144 bases in length, extending from the junction of R/U5 and U5/L stem-loops to the end of SL4. The *trans*-acting responsive element, polyadenylation signal, primer binding site, upper stem-loop of U5/L, and SL2 were not needed for the function of this region. The insertion of this region into the ectopic location of the viral genome did not affect the level of virion production by transfection. However, the resultant virions contained monomerized genomes and showed drastic reductions in infectivity. A reduction was observed especially in the reverse transcription process. An attempt to generate a replication-competent virus with monomerized genome was performed by the long-term culture of mutant virus-infected cells. All recovered viruses were wild-type revertants, indicating a fatal defect of the mutation. These results suggest that genome dimerization or DIS/DLS itself also plays an important role in the early stages of virus infection.

The retrovirus genome is a single-stranded, positive-sense RNA. The viral genome always occurs as a dimer in virus particles, and the interaction is noncovalent since heating easily dissociates purified dimeric genomes into monomers. Template strand switching between two genomes during reverse transcription is often observed in the retroviral life cycle (15). It is likely that the presence of two genomes in one virion helps the virus survive by providing an extra template that can be used when one RNA molecule is damaged and/or providing genetic variety for the progeny. However, this may not fully explain why the virion has to carry two identical RNAs in spite of severe space limitation, so the precise nature of retroviral genome dimerization is still unclear.

The identification of *cis*-acting signals for retrovirus genome dimerization was initially attempted in an in vitro assay (10, 11, 21, 34, 36). Synthesized 5′ RNA fragments of a viral genome, with a length of several hundred to a thousand bases, were found to be dimerized by heating and cooling under suitable buffering conditions. The proposed dimer initiation site/dimer linkage sequence (DIS/DLS) region of human immunodeficiency virus type 1 (HIV-1) is located within the untranslated region between the long terminal repeat (LTR) and the *gag* gene (11, 22). As these regions overlap with a packaging signal, however, it was difficult to perform mutational analysis to study the dimerization of the genome within the virion. Therefore, we recently developed a system to assess the dimerization signal operating within the HIV-1 virion without affecting the packaging ability of the genome (41). This system is an application of our previous finding that duplication of the encapsidation/dimerization signal (E/DLS) region on one RNA genome resulted in the appearance of a monomeric genome in the HIV-1 virion (40). We speculated that an additional E/DLS region at the ectopic position binds to the authentic E/DLS region on the same RNA molecules, thus competitively interfering with intermolecular dimer formation (Fig. 1A). Mutational analysis could thus be utilized to map the DIS/DLS precisely on the HIV-1 RNA. By applying this system, part of the 5′ untranscribed region (UTR) of the HIV-1 genome was examined, and separate functional maps for dimerization and encapsidation signals could be created. By comparing these two maps, we concluded that RNA dimer linkage formation must be an essential process in genome packaging, which consists of multiple sequential steps (41). In the study reported here, we employed our original system to identify the region which is necessary and sufficient for HIV-1 genome dimerization in the virion. We also report on our further investigation of the roles of the dimerization signal at various stages of viral replication and discuss the possibility that it may perform functions other than genome packaging in the viral life cycle.

MATERIALS AND METHODS

DNA constructs. The replication-competent HIV-1 proviral clone pNL4-3 (2) and pMSMBA (23), a derivative of pNL4-3, were used as progenitors for the mutant constructs described here. Mutant plasmids were constructed with standard methods. To construct pDDNT4, pDDNU4, and pDDNL4, three pairs of primers were first used for PCR amplification of the HIV-1 leader region by using the plasmid pGEM-MM (40) as a template. The first pair comprised the sense primer TarF (5′-GGTCTCTCTGGTTAGACCAG-3′) and the antisense primer SL4Rs (5′-GACGCTCTCGCACCCATC-3′), the second pair consisted of the sense primer R/U5F (5′-CACTGCTTAAGCCTCAACGATCG-3′) and the antisense primer SL4Rs, and the third pair consisted of the sense primer

* Corresponding author. Mailing address: Department of Viral Infections, Research Institute for Microbial Diseases, Osaka University, 3-1 Yamadaoka, Suita City, Osaka 565-0871, Japan. Phone: 81-6-6879-834. Fax: 81-6-6879-8347. E-mail: sakuragi@biken.osaka-u.ac.jp.

[▽] Published ahead of print on 15 May 2007.

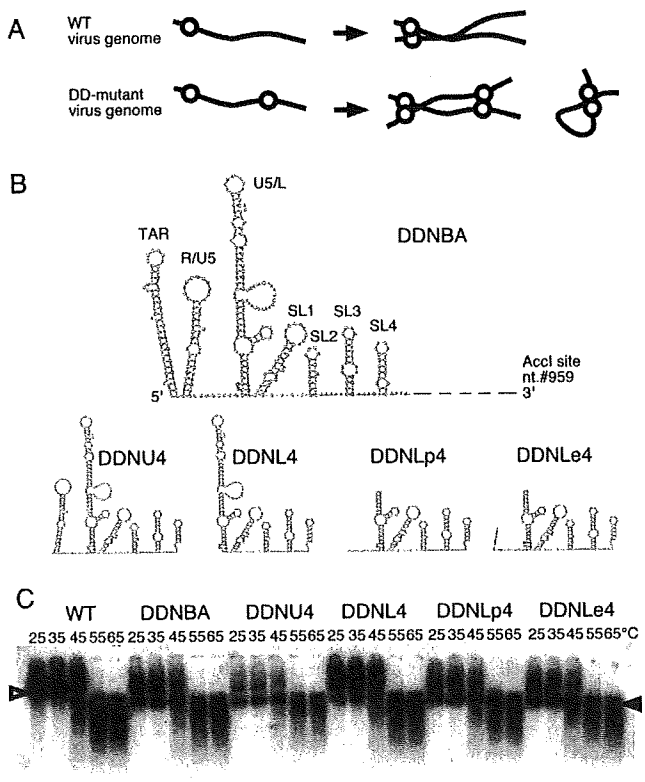

FIG. 1. The 5′ and 3′ ends of a functional domain of DLS. (A) A schematic image of monomer formation of the E/DLS duplicated mutant (DD-mutant) genome. Genomes of the WT virus form dimers, whereas those of DD-mutant form both dimers and monomers. Solid lines and open circles represent viral genome RNA and E/DLS, respectively. (B) Possible two-dimensional folds of the inserted fragment of each of the constructed mutants. nt., nucleotide. (C) Virion RNA profiles in native agarose gel. Viruses were prepared by transfection of 293T cells with pNLNh (WT) or its derivative mutants. At 48 h posttransfection, culture supernatants were harvested. Virions in the supernatant were collected by ultracentrifugation through a 20% sucrose cushion for isolation of the virion RNA. Open and solid arrowheads denote positions of dimers and monomers, respectively.

U5/LF (5′-TCTGTTGTGTGACTCTGGTAAC-3′) and the antisense primer SL4Rs. The three amplified fragments were isolated and ligated in pGEM-Teasy (Promega, Madison, WI) to generate pGEMT4sub, pGEMU4sub, and pGEML4sub, respectively. The digestion of these plasmids with EcoRI, blunt ended by T4 DNA polymerase, resulted in the isolation of approximately 300-bp fragments, including the 5′ leader region of HIV-1. These fragments were then ligated into the T4 DNA polymerase-treated NheI site of pNL4-3 to construct pDDNT4, pDDNU4, and pDDNL4, respectively. The orientation of the inserted fragments was verified by sequencing. pDDNLp4 and pDDNLe4 were constructed in a similar way, except for the use of pdLA3 (39) as a PCR template and different sense primers. The sense primer for pDDNLp4 was A3F+N (5′-TGTGCCCGTCTGTTGTGTGACTC-3′), and that for pDDNLe4 was A3U5endN (5′-AGTAGTGTGTGCCCGTCTGTTGTGTGACTC-3′). To construct pDDNLp4Δ1 and pDDNLp4Δ3, pdM and pdX (25) were used as templates for PCR amplification with the sense primer LpLA3 (5′-TGTGCCCGTCTGTTGTGTGACTCTGGTGCCAGAGGAG-3′) and the antisense primer SL4Rs, respectively. The two amplified fragments were isolated and ligated in pGEM-Teasy to generate pGEMLp4Δ1sub and pGEMLp4Δ3sub, respectively. To construct pDDNLp4Δ2, two-step PCR amplification was performed by using pGEMLp4sub as a template. The first pair of primers comprised the sense primer A3F+N and the antisense primer dS2R (5′-CAAAATTTTTGCCCCTCGCC-3′), and the second pair comprised the sense primer dS2F (5′-GGCGAGGGGCAAAAATTTTG-3′) and the antisense primer SL4Rs. Two amplified fragments were isolated, mixed, and used for the second PCR with primers A3F+N and SL4Rs to generate a mutated fragment. This fragment was then isolated and ligated in pGEM-Teasy to generate pGEMLp4Δ2sub. To construct pDDNLp4Δ4, pGEMLp4sub was used as a template for PCR amplification with the sense primer A3F+N and the antisense primer dS4 (5′-CATCTCTCCTTCTAGCC-3′). The amplified fragment was isolated and ligated in pGEM-Teasy to generate pGEMLp4Δ4sub. The digestion of pGEMLp4Δ1sub, -Δ2sub, -Δ3sub, and -Δ4sub with EcoRI, blunt ended by T4 DNA polymerase, resulted in the isolation of fragments, including the 5′ leader region of HIV-1. These fragments were then ligated into the T4 DNA polymerase-treated NheI site of pNL4-3 to construct pDDNLp4Δ1, -Δ2, -Δ3, and -Δ4, respectively. The EcoRI fragment from pGEMLp4Δ2sub (fragment Lp4Δ2) was blunt ended by T4 DNA polymerase and ligated into the BsaBI site of pDDNLp4Δ2 to create pDTNLp4Δ2. The plasmid p5′ssβglob (24) features a deletion on the 5′ untranslated region of pMSMBA (nucleotides 694 to 783) and an insertion at the point of deletion of a portion of the sequence spanning the 5′ splicing signal of the first intron of the β-globin gene. The 2.2-kb StuI-XhoI fragments containing env regions of pDDNLp4Δ2 and pDTNLp4Δ2 were inserted into the corresponding position of p5′ssβglob to create pssNLp4Δ2 and psTNLp4Δ2, respectively. The fragment Lp4Δ2 was blunt ended by T4 DNA polymerase and ligated into the T4 DNA polymerase-treated XhoI site of pNL4-3 to construct pDDXE+. The fragment Lp4Δ2 was ligated into the EcoRI site of pNL4-3 to construct pDDEE+. pDDEE+ was digested with Sse8387I, and NheI, a 4.4-kb, *pol-env* region-containing fragment, was isolated and exchanged at the same position of pDDXE+ to construct pDTEXE+. The construction of the HIV-2 *env* expression vector, pCGH2env, has been described previously elsewhere (28).

DNA transfection. 293T cells (13) (approximately 3×10^6) were seeded on dishes (diameter, 100 mm) the day before transfection with plasmid DNA (5 μg) by means of the calcium phosphate precipitation method (3). The day after transfection, the supernatant was replaced with fresh medium.

Virus infection. At 48 to 72 h posttransfection, the medium was centrifuged and the supernatant was used for infection with inoculation of equal amounts of CA-p24 into MT-4, M8166, or M8166/H1Luc cells (27). The supernatants of MT-4 or M8166 were harvested every 3 or 4 days for the multiple replication assay, while 10 μl of each cell supernatant was analyzed with the exogenous reverse transcriptase (RT) assay as described previously (43). M8166/H1Luc cells contain integrated reporter DNA carrying the HIV-1 LTR and luciferase. Upon infection with HIV-1, the HIV-1 LTR is activated along with the expression of viral transactivator Tat and luciferase expression in cytoplasm is induced. The same amount of CA-p24 recovered from each construct was inoculated into M8166/H1Luc cells, and luciferase expression within the cells was measured 24 h after infection. The luciferase assay was performed with the Bright-Glo luciferase assay system (Promega).

Isolation of RNA from virions. At 48 to 72 h posttransfection, virus particles were collected concurrently from medium as described previously elsewhere (23). The physical virus titer was determined with an enzyme-linked immunosorbent assay kit to quantitate CA-p24 (ZeptoMetrix, Inc., Buffalo, NY). To isolate RNA from particles, virions were disrupted by the addition of 1% sodium dodecyl sulfate and treated with proteinase K (300 μg/ml) at room temperature for 60 min, followed by Tris-EDTA-saturated phenol-chloroform extraction, chloroform extraction, and ethanol precipitation.

Northern blotting analysis. Pelleted RNA was resuspended in T buffer (10 mM Tris-HCl, pH 7.5, 1 mM EDTA, 1% sodium dodecyl sulfate, 100 mM NaCl, and 10% formamide), and the thermostability of dimeric viral RNA was determined by incubating RNA aliquots for 10 min at the temperatures indicated (42). RNA electrophoresis on native agarose gel and Northern hybridization analysis were performed as described previously elsewhere (41). Plasmid T7pol (42) was used to synthesize a cRNA probe for Northern hybridization. In experiments designed to assess the conversion of dimers to monomers, relative amounts of both RNA species were quantitated by PhosphorImager analysis (Fujifilm Co., Tokyo, Japan) and ratios of dimers and monomers were determined.

RNase protection assay. The antisense probe ($\sim 10^8$ cpm/mg) specific to the NL4-3 *gag* region was synthesized by in vitro transcription. One-fifth of the virion-associated RNA was mixed with 8×10^4 Cerenkov counts of ^{32}P-labeled antisense riboprobe and precipitated with ethanol. RNase protection assays were performed with an RPA III RNase protection assay kit (Ambion, Inc., Austin, TX). After electrophoresis in 5% polyacrylamide-8 M urea gels, protected RNA was quantitated by PhosphorImager analysis (Fujifilm Co.).

Real-time PCR analysis. At 48 to 72 h posttransfection, culture supernatants of the transfected cells were harvested. The supernatants were treated with DNase prior to infection to eliminate plasmid DNA contamination as described previously elsewhere (20) and inoculated into 10^6 MT-4 cells. For PCR analysis, total DNA was extracted from infected cells 20 h after infection by using a GenElute mammalian genomic DNA miniprep kit (Sigma, St. Louis, MO).

TABLE 1. Packaging efficiency of the mutants analyzed[a]

Mutant or WT	Avg ± SEM
WT	1 ± 0
DDNT4	0.84 ± 0.14
DDNU4	1.61 ± 0.26
DDNL4	1.09 ± 0.10
DDNLp4	1.04 ± 0.08
DDNLe4	0.94 ± 0.09

[a] The values were calculated by dividing the quantity of viral RNA by that of CA-p24. The value of WT (NLNh) was set at 1. Values are averages of results of at least three independent experiments.

Real-time PCR was performed with an Applied Biosystems 7500 real-time PCR system to quantitate viral cDNA synthesis during infection. Primers and TaqMan probes were selected according to criteria described previously elsewhere (19), and samples (0.5 μg DNA) were subjected to 40 cycles of PCR in a 10-μl reaction mixture. A series of known amounts of plasmid DNA were amplified along with total DNA to serve as a standard in each experiment. For the quantitation of the 2-LTR from virus DNA, a 2-LTR circle junction was cloned into pGEM-Teasy plasmid (Promega) as a TA cloning fragment by PCR amplification from 2-LTR circles, with total DNA extracted from infected MT-4 cells serving as a template. Serial dilutions of this plasmid were used as a standard to determine copy numbers of 2-LTR circles in the samples in the same manner as that for the determination of other DNA copy numbers.

For integrated proviral DNA quantitation, a modification of a recently reported Alu PCR method (7, 18) was employed (28). In short, two outward-facing Alu primers that anneal within the conserved regions of the Alu repeat element were used, together with an HIV-1 LTR-specific primer (L-M667), to optimize the probability of amplifying an LTR sequence for the first round of PCR. For the second round of PCR (real-time PCR), a lambda-specific primer (Lambda T) was used as a sense primer to detect only the amplified fragments in the first round of PCR and a TaqMan probe and an antisense primer were selected from the previous set for R/U5 DNA detection (19). The resultant PCR products were diluted 100-fold and subjected to real-time PCR.

RESULTS

The 5′ and 3′ ends of a functional domain of DIS/DLS. In a previous study of ours, the minimal RNA region required for RNA dimerization in virions was identified as a fragment inserted in the *env* region of pDDNBA (41). The fragment was approximately 500 bases long, extending from the 5′ capping site to the middle of the MA gene of the viral genome with deletion of the polyadenylation signal and primer binding site (PBS). We first constructed five mutants to precisely map the 5′ and 3′ ends of the functional region of DIS/DLS (Fig. 1). The viral genome packaging efficiency of all mutants was similar to that of the wild type (WT), indicating that the mutations had little effect on packaging ability (Table 1). The viral genome from mutant DDNT4, which contains an ectopic fragment (334 bases, from the *trans*-acting responsive element [TAR] to SL4) at the *env* region, formed a monomer very similar to that of the original mutant DDNBA (monomer content was more than 40% of the total viral genome in native condition), which indicated that sequence 3′ to SL4 was not needed for mediating RNA-RNA interactions in virions (data not shown). pDDNU4 carried a fragment from the R/U5 [poly(A)] stem-loop to SL4 (277 bases), and pDDNL4 carried a fragment from the U5/L stem-loop to SL4 (222 bases). As shown in Fig. 1B, the viral genome from DDNU4 formed a monomeric RNA comparable to DDNBA (monomer content was more than 40%), whereas the viral genome from DDNL4 formed a monomeric RNA with a greatly reduced amount of monomer (<20%). These results indicate that the 5′ end of the functional region of DIS/DLS was lost from DDNL4. We therefore added 8 and 15 nucleotides of the 5′ sequences to DDNL4 to generate DDNLp4 and DDNLe4, respectively. An upper stem-loop and PBS of the U5/L region were deleted from the inserted fragment of DDNLp4 and DDNLe4 because our previous data showed that those parts were dispensable for the dimer linkage formation function (41). Both viral RNAs of DDNLp4 and DDNLe4 formed a genome with a monomeric content (>40%) comparable to that of the WT in the virion (Fig. 1B). Taken together, these findings suggest that the region from the R/U5-U5/L junction to SL4 is sufficient to produce dimeric RNA in virions.

Minimal region sufficient for RNA dimerization is 144 bases long. We then examined the involvement in dimer linkage formation of four stem-loops, SL1 (putative "DIS"), SL2 (splicing signal), SL3 (essential region of packaging signal), and SL4 (containing *gag*AUG). Four mutants, DDNLp4Δ1, DDNLp4Δ2, DDNLp4Δ3, and DDNLp4Δ4, were constructed as derivatives of DDNLp4. Each mutant contained a deletion of one of four stem-loops on the ectopic fragment of DDNLp4 (Fig. 2A). As shown in Fig. 2B, only DDNLp4Δ2 formed a monomeric genome similar to the one derived from DDNBA,

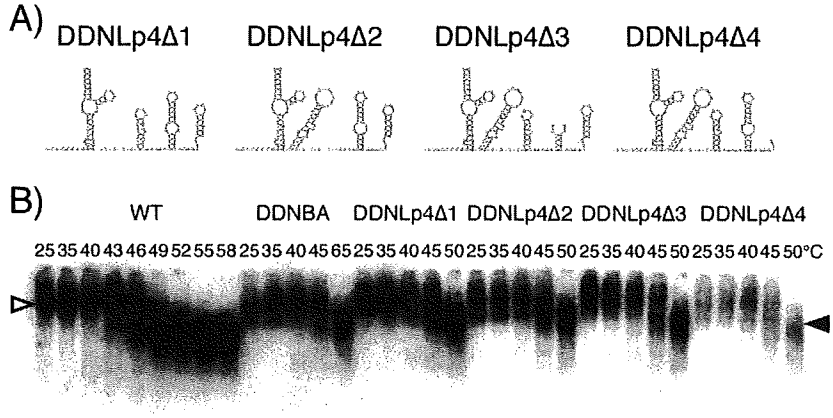

FIG. 2. Determination of the necessary and sufficient DLS in virions. (A) Probable two-dimensional folds of the inserted fragment of each of the constructed mutants. (B) Virion RNA profiles in native agarose gel. Virion RNA was isolated, and Northern hybridization was performed as described for Fig. 1. Open and solid arrowheads denote positions of dimers and monomers, respectively.

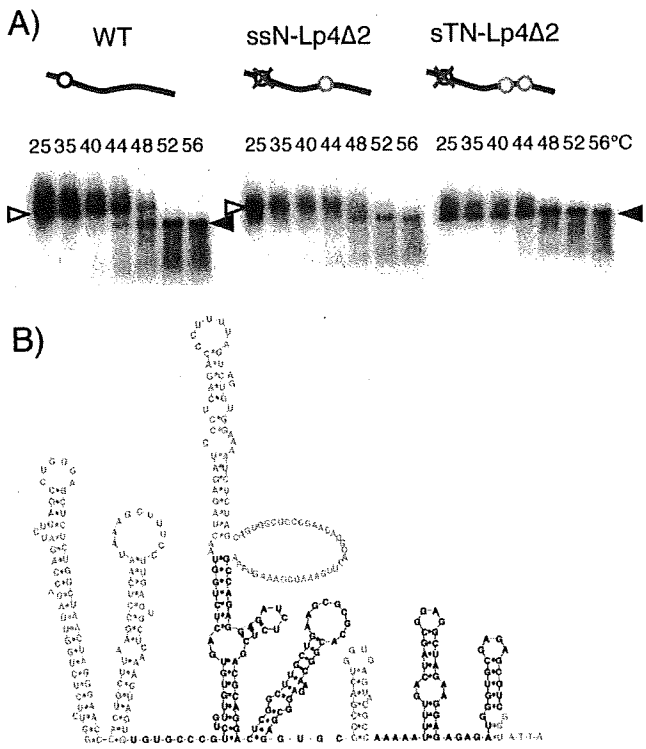

FIG. 3. Verification of the minimal DLS for its ability to induce RNA-RNA interaction in HIV-1 virions. (A) Virion RNA profiles in native agarose gel. Virion RNA was isolated, and Northern hybridization was performed as described for Fig. 1. Open and solid arrowheads denote positions of dimers and monomers, respectively. Schematic diagrams of mutants are shown above the blots. Solid lines, open circles, gray circles, and gray crosses represent viral genome RNA, authentic E/DLS, Lp4Δ2 fragments, and mutations introduced to knock out E/DLS functions, respectively. (B) A schematic Mfold representative of the verified area.

whereas other mutants displayed low levels of monomeric genome formation in virions. This indicates that the major splicing donor, SL2, is dispensable for RNA-RNA interaction, while the three other stem-loops are necessary for dimer linkage formation in virions.

In a previous study, we constructed two mutants, ssN− and sTN−, which contained a deletion of authentic DIS/DLS and an insertion of one (ssN−) or two (sTN−) DIS/DLS fragments in the ectopic position of the viral genome (39). Viral genomes from dimers formed from ssN− were similar to the WT, and nearly all viral genomes in virions of sTN− were monomers. This suggests that the two fragments inserted on one RNA strand interacted exclusively and intramolecularly with each other to prevent intermolecular dimerization. To confirm that fragment Lp4Δ2 was necessary and sufficient for RNA dimer linkage formation in virions, we constructed two mutants, ssNLp4Δ2 and sTNLp4Δ2, in the same way that ssN− and sTN− were constructed, except for the use of fragment Lp4Δ2 for insertion. As we expected, viral genomes from ssNLp4Δ2 formed dimers similar to those of the WT, while the viral genome from sTNLp4Δ2 exclusively formed monomers (Fig. 3A). Thus, the Lp4Δ2 fragment, 144 bases in length, was necessary and sufficient for mediating RNA dimerization in HIV-1 virions (Fig. 3B).

Single-round infection efficiency of HIV-1 mutant containing monomeric genome. We previously demonstrated the particle formation of HIV-1 which contained exclusively monomerized genome (39). This suggested that whole-genome dimerization is not essential for RNA packaging and particle formation of the viral genome, although dimer linkage formation of the DLS region is essential for these functions (41). On the other hand, no efficient infection or replication of HIV-1 mutants containing a monomeric genome was observed since significant reduction of intact viral DNA production occurred as a result of aberrant strand transfer and/or recombination during reverse transcription (39). Strand transfer during the reverse transcription process of the retroviral genome targets the R region of the viral LTR (12), which has also been suggested to be a hot spot for recombination (26). The production of aberrant viral cDNA products could thus be induced by the presence of multimerized R regions on the genome of the mutants. Since Lp4Δ2, the minimum DLS we identified here, did not include any R region, its ability to induce aberrant strand transfer and/or recombination by duplication of Lp4Δ2 in the viral genome was expected to be reduced. We therefore compared the single-round replication efficiencies of mutants DDNLp4Δ1, -Δ2, -Δ3, and -Δ4 pseudotyped with the HIV-2 envelope. The result demonstrated that all mutants containing Lp4 fragments showed reduced infectivity, which may be the effect of homologous recombination at a sequence-duplicated location (Fig. 4A). However, the infectivity of DDNLp4Δ2, the only mutant packaging monomeric genome, was three- to five-fold lower than that of other mutants. As the M8166/H1Luc cell assay reflects the magnitude of Tat expression of the samples, this result suggests that the mutations introduced in these constructs affect mainly the step(s) between virus penetration and early gene expression.

Reverse transcription predominantly blocked in monomeric genome mutants. To determine the step(s) in the viral replication cycle affected by the mutation described above, we analyzed the efficiency of each of the replication steps of the mutants. We chose two mutants, DDNLp4Δ2 and -Δ3, for comparison, since they are very similar in length of duplicated sequences but quite different in infectivity. We analyzed the virion production and viral RNA encapsidation ability of the mutants by purifying the virion and viral RNA from the supernatant of transfectant 293T cells. As shown in Fig. 4B, both functions of the mutants were similar or only moderately reduced compared to those of the WT, indicating that the mutations had little effect on these processes.

We next quantitated the levels of virus reverse-transcribed products, 2-LTR viral circular DNA, and integrated viral DNA using real-time PCR. HIV-2 *env*-pseudotyped virus was generated by transfection and purified, and equivalent amounts of CA-p24 were used to infect MT-4 cells. At 20 h after infection, total DNA was isolated from virus-infected cells. To examine the progress of reverse transcription, four sets of primers and probes were prepared (see Materials and Methods) and used to measure the synthesis of the strong-stop negative-strand DNA, first-strand transferred DNA, *gag* region DNA, and second-strand transferred DNA within total cellular DNA. Figure 4C shows the organized results of viral DNA quantitation.

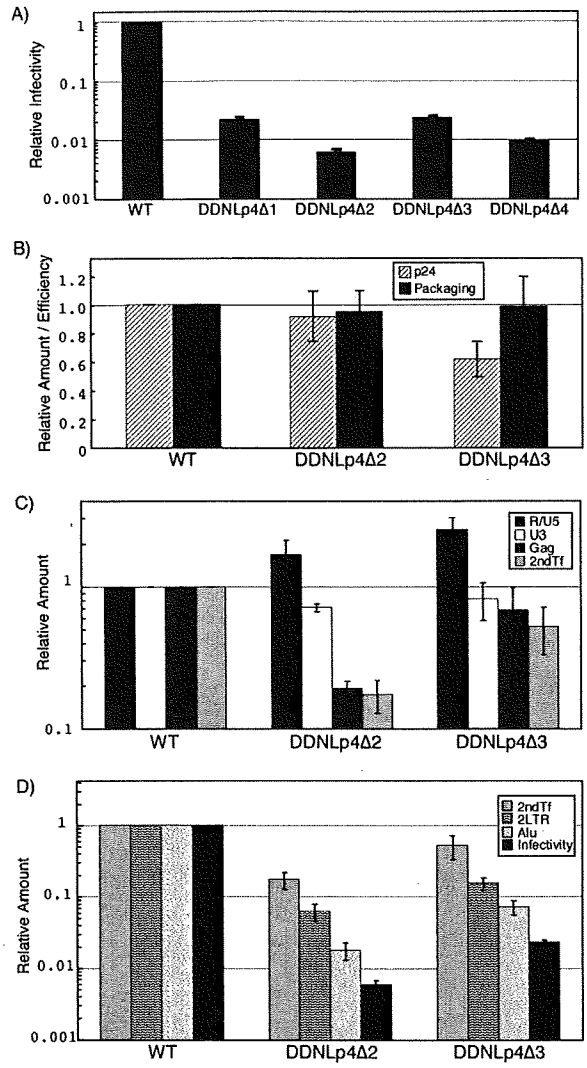

FIG. 4. Infectivity of mutant viruses. For each graph, the value of the WT was set at 1. Figures show the averages of results of at least two independent experiments. Error bars represent standard errors. (A) Single-round replication assay. M8166/H1Luc cells (1×10^6) were infected with the same quantity of CA-p24 of WT or mutant viruses pseudotyped with HIV-2 Env. At 24 to 48 h postinfection, cells were lysed and luciferase activity in the cell lysate was measured. (B) CA-p24 production and RNA packaging ability. Quantities of CA-p24 and viral RNA of purified virions were measured with the enzyme-linked immunosorbent assay and the RNase protection assay, respectively. Packaging efficiency was calculated by dividing the quantity of viral RNA by that of CA-p24. (C and D) Viral DNA quantification at early infection steps. A total of 1×10^5 MT-4 cells were infected with the same quantity of CA-p24 of WT or mutant viruses pseudotyped with HIV-2 Env. At 20 h postinfection, total cellular DNA was extracted and treated with DpnI overnight to digest methylated plasmid DNA. An equal amount of DNA was subjected to real-time PCR analysis. R/U5, strong-stop DNAs; U3, first-strand transferred products; Gag, negative-strand late products; 2ndTf, second-strand transferred products; 2LTR, 2-LTR viral circular DNA; Alu, PCR quantification for integrated proviral DNA; Infectivity, M8166/H1Luc cell assay as described for Fig. 4A.

Compared to the WT, a moderately large amount of DNA of both mutants was observed at the point of strong-stop DNA synthesis, which was reduced to a level similar to that of the WT in the subsequent first-strand transfer. At the next step, a big difference between the two mutants was observed. During the elongation of negative-strand DNA, the level of DNA synthesis of the DDNLp4Δ2 mutant was reduced to about 20%, whereas that of the DDNLp4Δ3 mutant remained at more than 60%. The level of DNA after the second-strand transfer showed additional moderate reduction for both of the mutants. As a result, a less than 50% reduction in overall viral cDNA production was observed in the DDNLp4Δ3 mutant, but a more than 80% reduction was observed in the DDNLp4Δ2 mutant. This result suggests that one of the defects was present at the reverse transcription stage. The reduction of the amounts of 2-LTR DNA, integrated DNA, and the infectivity are essentially similar between two mutants (Fig. 4D). As the 2-LTR circular DNA can be used as an indicator of RT completion and nuclear import of viral DNA (19), our findings suggest that the replication process from nuclear import to early gene expression was not specifically affected in a dimerization-defective mutant.

Attempt to generate replication-competent HIV-1 mutant containing monomeric genome. Multiround replication of a defective mutant virus sometimes results in the appearance of compensatory mutations to recover infectivity of the mutant without affecting viral RNA stability (38). Although we could not detect any efficient infectivity of mutant DDNLp4Δ2, we thought it might be possible to generate a replication-competent HIV-1 mutant containing a monomeric genome by means of long-term culture of infected cells. To verify this possibility, we constructed three mutants with Lp4Δ2 fragments on their genome, which retained all essential genes (*gag*, *pol*, *env*, *tat*, and *rev*) and important accessory genes (*vif* and *vpu*) but packaged the monomeric genome. Fragment Lp4Δ2 was inserted into *vpr*, *nef*, or both of pNL4-3 to construct pDDEE+, pDDXE+, and pDTEXE+, respectively (Fig. 5A). 293T cells were transfected with these constructs, the culture supernatants were harvested 2 to 3 days later, and the released virions collected. Roughly, the level of virion production by all three mutants was similar to that of the WT (data not shown). The genome from mutant virions contained 30 to 50% of monomeric genomes as shown by native Northern blotting analysis, thus confirming our previous observation (Fig. 5C). The mutants were examined for their ability to replicate in human $CD4^+$ cell lines MT-4 and M8166. Figure 6B shows the growth kinetics of the mutants in MT-4 cells. Mutant DTEXE+ was replication defective in MT-4 cells, while two mutants, DDEE+ and DDXE+, showed detectable virus replication but with growth kinetics that were significantly reduced and delayed compared to those of WT. On the other hand, all mutants were replication negative in M8166 cells (data not shown). Replicated viruses in the culture supernatant of MT-4 were harvested at their kinetic peak point. Equal amounts of RT units of virus samples were used for assay of reinfection of MT-4 cells, the remainder was centrifuged to purify virions, and the viral genome RNA was isolated. Growth kinetics of reinfected mutants restored their replication ability to a level comparable to that of the WT, suggesting that they had become revertants (data not shown). The results of native Northern blotting of genome RNA showed that MT-4 replicating mutants formed mostly dimers similar to that of the WT (Fig. 5D). Proviral genome sequencing from infected MT-4 chromosomal DNA proved that Lp4Δ2 sequences inserted in ectopic positions of the genome

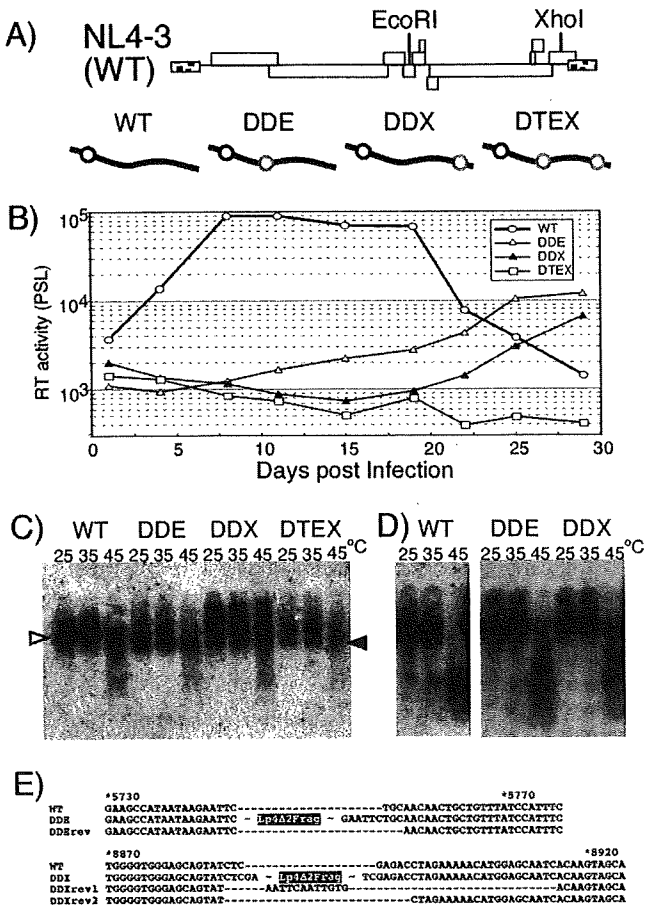

FIG. 5. Replication assay of mutants carrying a monomeric genome. (A) Schematic diagrams of replication-competent form mutants. The positions of restriction enzyme sites on the viral genome used for insertion are shown in the upper part of the panel. Diagrams of the mutants are shown in the lower part of the panel. Symbols are the same as those described for Fig. 3. (B) Growth kinetics of viruses. Values are representative of the results of at least three independent experiments. Viruses were prepared by transfection of 293T cells with pNL4-3 (WT) or its derivative mutants (pDDEE+ [DDE], pDDXE+ [DDX], and pDTEXE+ [DTE]). At 48 h posttransfection, culture supernatants of transfected 293T cells were harvested, and equal quantities of CA-p24 were inoculated into MT-4 cells. The supernatants of the cells were harvested every 3 or 4 days. Ten microliters of each cell supernatant was subjected to exogenous RT assay and quantitated by PhosphorImager analysis. PSL, Photostimulierte Lumineszenz. (C) Virion RNA profiles produced from transfected 293T cells and visualized by native Northern blotting analysis. Open and solid arrowheads denote positions of dimers and monomers, respectively. (D) Virion RNA profiles produced from MT-4 cells. Viruses were harvested at their growth kinetic peak point (wild type, 10 days postinfection; DDE and DDX, 28 days postinfection). (E) The nature of reversions. The sequences in the vicinity of the fragment-inserted sites are shown. The names of revertant sequences include "rev." The positions of Lp4Δ2 fragment insertion of DDE and DDX are indicated. The numbers above the sequences represent nucleotide positions of pNL4-3 (WT).

were completely deleted from both replication-competent mutants (Fig. 5E). Since the sequences of the revertants were found to contain an additional deletion or a small part of the inserted sequence at the mutated positions (Fig. 5E), the possibility of WT virus contamination could be ruled out.

DISCUSSION

The recent growth in interest in retrovirus genome dimerization has resulted in many publications that deal with its various aspects and that vary in depth and breadth (for reviews, see references 31, 35, and 37) Nonetheless, the overall picture of the retroviral dimerization signal remains unclear, so that there is still a need for detailed examination. The aim of the study reported here was to identify the minimal region sufficient for genome dimerization of HIV-1 in virions. In the first set of experiments, we defined the region sufficient for dimer linkage formation, and, in a subsequent experiment, we generated several deletion mutants to determine the minimal DLS required for HIV genome dimer linkage formation in virions. The minimal DLS identified in this study was only 144 bases long and included SL1, SL3, and SL4. Especially, SL1 deletion is more deleterious than is deletion of the other elements for dimer linkage formation in Fig. 2. It has been suggested that the hairpin loop of SL1 in DLS, known as DIS, plays a crucial role in dimerization and recombination (9, 33, 41). Our findings are well consistent with this notion.

While there are many functional regions for viral viability in the 5′ UTR of HIV, such as TAR, polyadenylation signal, PBS, and splicing donor, none was required for the dimerization function. This suggests that the genome dimerization of HIV-1 is independent of transactivation, splicing, or primer annealing. As we pointed out in a previous paper of ours (41) and in this study, the lower stem of the U5/L stem-loop is required for dimerization, which was not clearly identified during in vitro studies (for a review, see reference 30). This stem contains a so-called primer activation signal (5), which is thought to activate the initiation of reverse transcription. Since PBS or primer annealing is not required for dimerization, the involvement of primer activation signal and its opposing stem sequence in dimerization may be limited simply to creating a stable structure. Several studies have suggested that TAR, the R-U5 stem-loop region or coding region of *gag*, participates in the dimerization (4, 14, 16, 32) The contribution of those regions to RNA dimerization was demonstrated mainly in in vitro assays, but they were not included in the DLS identified in the in vivo assay used in our study. However, the possibility of a contribution by these regions cannot be ruled out since all mutants in our study retained the intact 5′ UTR. This result means that all mutants possess at least one set of the regions in the original position per genome, so that they may perform certain incidental functions for dimerization in virions.

Mfold RNA stability calculation (44) showed that the junction between R/U5 and U5/L stem-loops is relatively "free," which suggests that it is not involved in a base-pairing interaction with vicinal sequences (Fig. 1A). However, recent reports have suggested that the HIV-1 genome leader region could form an alternative structure known as the branched multiple hairpin (BMH) (1, 17). In this model, the 5′ junction sequence forms a stem structure with a sequence at the 3′ end of DLS. Although the BMH model was validated in an in vitro experiment, the DLS we defined in vivo was found to include all sequences required for the BMH formation. As an interaction between 5′ and 3′ ends of DLS should be essential for BMH formation, we evaluated the importance of both ends in vivo by making several base substitution mutants. The mutants con-

tained four to eight-base substitutions in either or both ends of the Lp4Δ2 fragment inserted in pDDNLp4Δ2. As expected, the 5′ or 3′ region of DLS appeared to be very important in dimer linkage formation of RNA since at least four-base substitutions (four substitutions in 8 bases of the 5′ end or four substitutions in 15 bases of the 3′ end) seriously disrupted the function (data not shown). Nonetheless, our attempt failed to yield a clear answer to whether BMH structure exists in virion RNA, probably because of difficulty in estimating the effect of the mutations on actual RNA shape in this region.

A noteworthy result of the M8166/H1Luc cell assay, an infectivity assay of monomeric genome mutants, was that the overall single-round infectivity of the mutant DDNLp4Δ2 was dramatically reduced (Fig. 4A). In our previous study, we reported that another monomeric genome mutant, DDNΔPBS, produced virions with less than 1% of infectivity of the WT (in one representative experiment, 1.4 versus 187.5 β-galactosidase-inducing units per ng of CA-p24 in a multinuclear activation of galactosidase indicator cell assay) (39). It well coincided with the data we got in the present study. As the inserted fragments of the four mutants were very similar in length and sequence (DDNLp4Δ1, 128 bases; DDNLp4Δ2, 144 bases; DDNLp4Δ3, 149 bases; and DDNLp4Δ4, 149 bases), a prominent replication defect of DDNLp4Δ2 might correlate with the appearance of monomeric genomes in virions, which is a unique feature of this mutant. Stepwise measurement of replication efficiency identified defects of the mutants in multiple steps of infection (Fig. 4C and D). Levels of viral DNA synthesis of DDNLp4Δ2 fell to around 15% of WT, whereas more than half of its viral DNA synthesis ability was retained in the DDNLp4Δ3 mutant. This difference strongly suggests a negative effect of the monomeric genome on reverse transcription. As the monomeric genome in virions of DDNLp4Δ2 accounted for 50% or less (Fig. 2B) of their content, the defect shown here occurred not only on the monomeric genome but also on the normal-looking dimeric genome of the mutants. These results seem to indicate that the inserted fragment of the mutant caused an abnormal secondary or tertiary structure of the overall viral RNA genome, resulting in poor reverse transcription. Viral genome dimerization and/or DIS was reported to play a role in efficient reverse transcription (6, 29), and our data supported these earlier arguments.

A multiround infection experiment clearly demonstrated significantly reduced growth kinetics of the mutants (Fig. 5). Moreover, inserted sequences of the mutants were completely deleted during the replication process, which strongly suggests that the insertion caused a fatal defect in viral replication. The appearance of revertants before the occurrence of compensation mutation implies that aberrant viral RNA conformation in these mutants was too drastic to be undone by protein modification.

In conclusion, in this study, we succeeded in identifying the essential region for HIV-1 genome dimer linkage formation in virions. Our consecutive experiments demonstrated that the dimerization region on RNA molecules may be important for the efficient progress of reverse transcription, probably by maintaining an appropriate form of viral genome in virions. A recent study has suggested that HIV-1 *pol* proteins contribute to genome RNA dimerization (8), which could be related to our speculation. Further studies can be expected to provide more findings relevant to this hypothesis.

ACKNOWLEDGMENTS

This work was supported by grants from the Ministry of Education, Culture, Sports, Science and Technology; the Ministry of Health, Labor, and Welfare; and the Health Science Foundation of Japan.

REFERENCES

1. **Abbink, T. E., and B. Berkhout.** 2003. A novel long distance base-pairing interaction in human immunodeficiency virus type 1 RNA occludes the Gag start codon. J. Biol. Chem. **278:**11601–11611.
2. **Adachi, A., H. E. Gendelman, S. Koenig, T. Folks, R. Willey, A. Rabson, and M. A. Martin.** 1986. Production of acquired immunodeficiency syndrome-associated retrovirus in human and nonhuman cells transfected with an infectious molecular clone. J. Virol. **59:**284–291.
3. **Aldovini, A., and B. D. Walker.** 1990. Techniques in HIV research. Stockton Press, New York, NY.
4. **Andersen, E. S., S. A. Contera, B. Knudsen, C. K. Damgaard, F. Besenbacher, and J. Kjems.** 2004. Role of the trans-activation response element in dimerization of HIV-1 RNA. J. Biol. Chem. **279:**22243–22249.
5. **Beerens, N., F. Groot, and B. Berkhout.** 2001. Initiation of HIV-1 reverse transcription is regulated by a primer activation signal. J. Biol. Chem. **276:** 31247–31256.
6. **Berkhout, B., A. T. Das, and J. L. van Wamel.** 1998. The native structure of the human immunodeficiency virus type 1 RNA genome is required for the first strand transfer of reverse transcription. Virology **249:**211–218.
7. **Brussel, A., and P. Sonigo.** 2003. Analysis of early human immunodeficiency virus type 1 DNA synthesis by use of a new sensitive assay for quantifying integrated provirus. J. Virol. **77:**10119–10124.
8. **Buxton, P., G. Tachedjian, and J. Mak.** 2005. Analysis of the contribution of reverse transcriptase and integrase proteins to retroviral RNA dimer conformation. J. Virol. **79:**6338–6348.
9. **Chin, M. P., T. D. Rhodes, J. Chen, W. Fu, and W. S. Hu.** 2005. Identification of a major restriction in HIV-1 intersubtype recombination. Proc. Natl. Acad. Sci. USA **102:**9002–9007.
10. **Darlix, J. L., C. Gabus, and B. Allain.** 1992. Analytical study of avian reticuloendotheliosis virus dimeric RNA generated in vivo and in vitro. J. Virol. **66:**7245–7252.
11. **Darlix, J. L., C. Gabus, M. T. Nugeyre, F. Clavel, and F. Barre-Sinoussi.** 1990. *cis* elements and *trans*-acting factors involved in the RNA dimerization of the human immunodeficiency virus HIV-1. J. Mol. Biol. **216:**689–699.
12. **Götte, M., X. Li, and M. A. Wainberg.** 1999. HIV-1 reverse transcription: a brief overview focused on structure-function relationships among molecules involved in initiation of the reaction. Arch. Biochem. Biophys. **365:**199–210.
13. **Graham, F. L., J. Smiley, W. C. Russell, and R. Nairn.** 1977. Characteristics of a human cell line transformed by DNA from human adenovirus type 5. J. Gen. Virol. **36:**59–74.
14. **Höglund, S., Å. Öhagen, J. Goncalves, A. T. Panganiban, and D. Gabuzda.** 1997. Ultrastructure of HIV-1 genomic RNA. Virology **233:**271–279.
15. **Hu, W. S., and H. M. Temin.** 1990. Retroviral recombination and reverse transcription. Science **250:**1227–1233.
16. **Huthoff, H., and B. Berkhout.** 2001. Mutations in the TAR hairpin affect the equilibrium between alternative conformations of the HIV-1 leader RNA. Nucleic Acids Res. **29:**2594–2600.
17. **Huthoff, H., and B. Berkhout.** 2001. Two alternating structures of the HIV-1 leader RNA. RNA **7:**143–157.
18. **Ikeda, T., H. Nishitsuji, X. Zhou, N. Nara, T. Ohashi, M. Kannagi, and T. Masuda.** 2004. Evaluation of the functional involvement of human immunodeficiency virus type 1 integrase in nuclear import of viral cDNA during acute infection. J. Virol. **78:**11563–11573.
19. **Julias, J. G., A. L. Ferris, P. L. Boyer, and S. H. Hughes.** 2001. Replication of phenotypically mixed human immunodeficiency virus type 1 virions containing catalytically active and catalytically inactive reverse transcriptase. J. Virol. **75:**6537–6546.
20. **Koh, K. B., M. Fujita, and A. Adachi.** 2000. Elimination of HIV-1 plasmid DNA from virus samples obtained from transfection by calcium-phosphate co-precipitation. J. Virol. Methods **90:**99–102.
21. **Marquet, R., F. Baudin, C. Gabus, J. L. Darlix, M. Mougel, C. Ehresmann, and B. Ehresmann.** 1991. Dimerization of human immunodeficiency virus (type 1) RNA: stimulation by cations and possible mechanism. Nucleic Acids Res. **19:**2349–2357.
22. **Marquet, R., J. C. Paillart, E. Skripkin, C. Ehresmann, and B. Ehresmann.** 1994. Dimerization of human immunodeficiency virus type 1 RNA involves sequences located upstream of the splice donor site. Nucleic Acids Res. **22:**145–151.
23. **McBride, M. S., and A. T. Panganiban.** 1996. The human immunodeficiency virus type 1 encapsidation site is a multipartite RNA element composed of functional hairpin structures. J. Virol. **70:**2963–2973.

24. **McBride, M. S., and A. T. Panganiban.** 1997. Position dependence of functional hairpins important for human immunodeficiency virus type 1 RNA encapsidation in vivo. J. Virol. **71**:2050–2058.
25. **McBride, M. S., M. D. Schwartz, and A. T. Panganiban.** 1997. Efficient encapsidation of human immunodeficiency virus type 1 vectors and further characterization of *cis* elements required for encapsidation. J. Virol. **71**: 4544–4554.
26. **Moumen, A., L. Polomack, B. Roques, H. Buc, and M. Negroni.** 2001. The HIV-1 repeated sequence R as a robust hot-spot for copy-choice recombination. Nucleic Acids Res. **29**:3814–3821.
27. **Nagao, T., A. Yoshida, A. Sakurai, A. Piroozmand, A. Jere, M. Fujita, T. Uchiyama, and A. Adachi.** 2004. Determination of HIV-1 infectivity by lymphocytic cell lines with integrated luciferase gene. Int. J. Mol. Med. **14**:1073–1076.
28. **Ohishi, M., T. Shioda, and J. I. Sakuragi.** 2007. Retro-transduction by virus pseudotyped with glycoprotein of vesicular stomatitis virus. Virology **362**: 131–138.
29. **Paillart, J. C., L. Berthoux, M. Ottmann, J. L. Darlix, R. Marquet, B. Ehresmann, and C. Ehresmann.** 1996. A dual role of the putative RNA dimerization initiation site of human immunodeficiency virus type 1 in genomic RNA packaging and proviral DNA synthesis. J. Virol. **70**:8348–8354.
30. **Paillart, J. C., R. Marquet, E. Skripkin, C. Ehresmann, and B. Ehresmann.** 1996. Dimerization of retroviral genomic RNAs: structural and functional implications. Biochimie **78**:639–653.
31. **Paillart, J. C., M. Shehu-Xhilaga, R. Marquet, and J. Mak.** 2004. Dimerization of retroviral RNA genomes: an inseparable pair. Nat. Rev. Microbiol. **2**:461–472.
32. **Paillart, J. C., E. Skripkin, B. Ehresmann, C. Ehresmann, and R. Marquet.** 2002. In vitro evidence for a long range pseudoknot in the 5′-untranslated and matrix coding regions of HIV-1 genomic RNA. J. Biol. Chem. **277**:5995–6004.
33. **Paillart, J. C., E. Skripkin, B. Ehresmann, C. Ehresmann, and R. Marquet.** 1996. A loop-loop "kissing" complex is the essential part of the dimer linkage of genomic HIV-1 RNA. Proc. Natl. Acad. Sci. USA **93**:5572–5577.
34. **Prats, A. C., C. Roy, P. A. Wang, M. Erard, V. Housset, C. Gabus, C. Paoletti, and J. L. Darlix.** 1990. *cis* elements and *trans*-acting factors involved in dimer formation of murine leukemia virus RNA. J. Virol. **64**:774–783.
35. **Rein, A.** 2004. Take two. Nat. Struct. Mol. Biol. **11**:1034–1035.
36. **Roy, C., N. Tounekti, M. Mougel, J. L. Darlix, C. Paoletti, C. Ehresmann, B. Ehresmann, and J. Paoletti.** 1990. An analytical study of the dimerization of in vitro generated RNA of Moloney murine leukemia virus MoMuLV. Nucleic Acids Res. **18**:7287–7292.
37. **Russell, R. S., C. Liang, and M. A. Wainberg.** 2004. Is HIV-1 RNA dimerization a prerequisite for packaging? Yes, no, probably? Retrovirology **1**:23.
38. **Russell, R. S., A. Roldan, M. Detorio, J. Hu, M. A. Wainberg, and C. Liang.** 2003. Effects of a single amino acid substitution within the p2 region of human immunodeficiency virus type 1 on packaging of spliced viral RNA. J. Virol. **77**:12986–12995.
39. **Sakuragi, J., A. Iwamoto, and T. Shioda.** 2002. Dissociation of genome dimerization from packaging functions and virion maturation of human immunodeficiency virus type 1. J. Virol. **76**:959–967.
40. **Sakuragi, J., T. Shioda, and A. T. Panganiban.** 2001. Duplication of the primary encapsidation and dimer linkage region of HIV-1 RNA results in the appearance of monomeric RNA in virions. J. Virol. **75**:2557–2565.
41. **Sakuragi, J., S. Ueda, A. Iwamoto, and T. Shioda.** 2003. Possible role of dimerization in human immunodeficiency virus type 1 genome RNA packaging. J. Virol. **77**:4060–4069.
42. **Sakuragi, J. I., and A. T. Panganiban.** 1997. Human immunodeficiency virus type 1 RNA outside the primary encapsidation and dimer linkage region affects RNA dimer stability in vivo. J. Virol. **71**:3250–3254.
43. **Willey, R. L., D. H. Smith, L. A. Lasky, T. S. Theodore, P. L. Earl, B. Moss, D. J. Capon, and M. A. Martin.** 1988. In vitro mutagenesis identifies a region within the envelope gene of the human immunodeficiency virus that is critical for infectivity. J. Virol. **62**:139–147.
44. **Zuker, M.** 1989. On finding all suboptimal foldings of an RNA molecule. Science **244**:48–52.

Targeted Delivery of Immunogen to Primate M Cells with Tetragalloyl Lysine Dendrimer[1]

Shogo Misumi,[2]* Mitsuaki Masuyama,[2]*† Nobutoki Takamune,* Daisuke Nakayama,* Ryotarou Mitsumata,* Hirokazu Matsumoto,* Norimitsu Urata,* Yoshihiro Takahashi,† Atsunobu Muneoka,† Takayuki Sukamoto,† Koichiro Fukuzaki,† and Shozo Shoji[3]*‡

Effective uptake of Ags by specialized M cells of gut-associated lymphoid tissues is an important step in inducing efficient immune responses after oral vaccination. Although stable nontoxic small molecule mimetics of lectins, such as synthetic multivalent polygalloyl derivatives, may have potential in murine M cell targeting, it remains unclear whether synthetic multivalent polygalloyl derivatives effectively target nonhuman and human M cells. In this study, we evaluated the ability of a tetragalloyl derivative, the tetragalloyl-D-lysine dendrimer (TGDK), to target M cells in both in vivo nonhuman primate and in vitro human M-like cell culture models. TGDK was efficiently transported from the lumen of the intestinal tract into rhesus Peyer's patches by M cells and then accumulated in germinal centers. Oral administration of rhesus CCR5-derived cyclopeptide conjugated with TGDK in rhesus macaque resulted in a statistically significant increase in stool IgA response against rhesus CCR5-derived cyclopeptide and induced a neutralizing activity against SIV infection. Furthermore, TGDK was specifically bound to human M-like cells and efficiently transcytosed from the apical side to the basolateral side in the M-like cell model. Thus, the TGDK-mediated vaccine delivery system represents a potential approach for enabling M cell-targeted mucosal vaccines in primates. ***The Journal of Immunology,*** **2009, 182: 6061–6070.**

Human immunodeficiency virus is transmitted primarily via the genital mucosa during sexual intercourse. Elucidating the early events in mucosally transmitted HIV-1 infection plays a critical role in characterizing the virus-host interactions and effective vaccine design and development. Mucosal transmission of HIV-1 infection is mediated by exposure to cell-free viruses and/or cell-associated viruses within mucosal secretions, and established within hours, and can be disseminated to draining lymph nodes within days (1, 2). Recent studies of pathological events in acute infection in nonhuman primates and humans have provided important insights into the disruption of the mucosal immune system. This disruption is evident in the rapid depletion of $CD4^+$ T cells within the GALT during acute infection (3, 4), suggesting that once mucosal infection has occurred, immune responses to infection are insufficient to prevent these events. Therefore, a preventive vaccine should effectively target the earliest events in the establishment of HIV infection at the mucosal site.

Conventional vaccines administered from any routes other than the oral route effectively induce protective systemic immune responses, but the level of protective immunity at the major site of HIV mucosal entry is less robust. However, neutralizing Abs administered i.v. at high doses can reach mucosal sites and block genital mucosal transmission of simian/HIV (SHIV)[4] in nonhuman primate models (5), suggesting that sufficient mucosal humoral immune responses induced by mucosal vaccines can prevent HIV infection. Some related studies have shown that mucosal vaccines induce not only secretory IgA at mucosal sites, but also mucosal cell-mediated immunity and systemic Abs against HIV (6–13). These studies suggest that mucosal vaccines have several advantages over conventional systemic vaccines because they can induce multi-immuno responses that prevent HIV infection at the mucosal site.

Current efforts to develop effective mucosal vaccines are mainly directed toward finding more efficient means of delivering appropriate Ags to the mucosal immune system and toward developing effective and safe mucosal adjuvants (14) because it has often proved difficult to stimulate strong mucosal IgA immune responses and protection against pathogens by mucosal administration of Ags without Ag delivery and adjuvant systems. It is generally accepted that M cells in Peyer's patches (PPs) are instrumental in initiating mucosal immunity against pathogens invading across epithelial barriers (15). The high transcytotic abilities of M cells

*Department of Pharmaceutical Biochemistry, Faculty of Medical and Pharmaceutical Sciences, Kumamoto University, Kumamoto, Japan; †Shin Nippon Biomedical Laboratories, Kagoshima, Japan; and ‡Kumamoto Health Science University, Kumamoto, Japan

Received for publication September 3, 2008. Accepted for publication March 13, 2009.

The costs of publication of this article were defrayed in part by the payment of page charges. This article must therefore be hereby marked *advertisement* in accordance with 18 U.S.C. Section 1734 solely to indicate this fact.

[1] This study was supported in part by a Grant-in-Aid for scientific research from the Ministry of Education, Culture, Sports, Science, and Technology of Japan, and a health science research grant from the Ministry of Health, Labor, and Welfare of Japan.

[2] S.M. and M.M. contributed equally to this work.

[3] Address correspondence and reprint requests to Dr. Shozo Shoji, Kumamoto University, Department of Pharmaceutical Biochemistry, Faculty of Medical and Pharmaceutical Sciences, 5-1 Oe-Honmachi, Kumamoto 862-0973, Japan. E-mail address: shoji@gpo.kumamoto-u.ac.jp

[4] Abbreviations used in this paper: SHIV, simian/HIV; DAPI, 4′,6-diamidino-2 phenylindole; DIC, differential interference contrast; DMF, dimethylformamide; EDS, energy-dispersive x-ray spectroscopy; FAE, follicle-associated epithelium; Fmoc, 9-fuorenylmethoxycarbonyl; GC, germinal center; PEG, polyethylene glycol; PP, Peyer's patch; PV, poliovirus; rcDDR5, rhesus CCR5-derived cyclopeptide; RT, room temperature; SMPD, synthetic multivalent polygalloyl derivative; TEM, transmission electron microscopy; TGDK, tetragalloyl-D-lysine dendrimer; TRITC, tetramethylrhodamine isothiocyanate; UEA-1, *Ulex europaeus agglutinin-1*; wpim, weeks postinitial immunization.

www.jimmunol.org/cgi/doi/10.4049/jimmunol.0802928

make them an attractive target for mucosally delivered vaccines because mucus secretion may flush away an applied mucosal vaccine at the mucosal site. Some studies showed that mucosal vaccine delivery can be improved using appropriate bioadhesin molecules such as lectins because M cell surface glycocalyx differs in carbohydrate composition from that of enterocytes in many species (16–22). *Ulex europaeus agglutinin-1* (UEA-1)-conjugated (23, 24) or σ1 protein-conjugated nasal vaccination (13, 25) induces not only strong Ag-specific mucosal IgA and plasma IgG responses, but also CTL immunity. However, lectins such as UEA-1 are of limited value in vaccine delivery because they are toxic and subject to intestinal degradation. Lambkin et al. (26) reported that a stable low m.w. four-copy gallic acid construct is a competitor of UEA-1 and appears to have high affinity for the fucose receptor on murine M cells. Although stable nontoxic small molecular mimetics of UEA-1 have the potential for M cell targeting in mice, it remains unclear whether these mimetics effectively target the nonhuman and human M cells.

In this study, we synthesized the tetragalloyl-D-lysine dendrimer (TGDK) and demonstrated its M cell targeting potential in both in vivo nonhuman primate and in vitro human M-like cell culture models.

Materials and Methods

TGDK and D-lysine dendrimer

The 9-fuorenylmethoxycarbonyl (Fmoc)-D-MAP_4-NH-(CH_2)-NH-Trt-resin (in this study referred to as Fmoc-D-lysine dendrimer resin; Watanabe Chemical Industries) was treated with 20% piperidine/dimethylformamide (DMF) for 20 min to remove the Fmoc group. To prepare TGDK, the resin (0.51 mmol) was then washed five times with DMF and reacted with 3,4,5-trimethoxybenzoic acid chloride (1 mmol) in triethylamine (7 mmol) at 40°C for 120 min. The resulting resin was washed with 1% triethylamine/DMF three times and DMF five times, and then treated with boron tribromide (the amount is 20× mole equivalent of that of DMF in the reaction mixture) at 40°C for 5 min before air drying. TGDK was extracted with Milli-Q water, purified, and lyophilized. The patent for the synthesis method of TGDK has been obtained (PCT/JP2006/321720). The D-lysine dendrimer was obtained by treating the D-lysine dendrimer resin with acetic acid/trifluoroethanol/dichloromethane (1:1:8). The molecular masses of TGDK and D-lysine dendrimer were determined by MALDI-TOF mass spectrometry (Burker Franzen Analytik).

Animals and tissue samples

Purpose-bred female rhesus macaques (*Macaca mulatta*) obtained from a supplier in China (4–6 years old) were used for this study. This study (permission no. 19-137) was approved and conducted in accordance with the guidelines of the Animal Care and Use Committee of Kumamoto University.

Inoculation of TGDK

Rhesus macaques were fasted overnight. They were then inoculated with 1 ml of FITC-labeled TGDK solution (100 nmol) or 0.5 ml of 10 nm gold-labeled TGDK at a site in the ileum (15 cm from the cecum) after celiotomy under anesthesia induced by a s.c. injection of urethane (ethyl carbamate, 800 mg/ml; 1.5 ml/kg body weight; Wako Pure Chemical) solution and an i.v. injection of α-chloralose (Wako Pure Chemical; 20 mg/ml; 5.5 ml/kg body weight) into the cephalic vein.

Inoculation of poliovirus (PV)

Rhesus macaques were fasted overnight. They were then inoculated with PV solution at a site in the ileum (15 cm from the cecum), as described previously (27).

Collection of PPs

The rhesus monkeys were euthanized by exsanguination under anesthesia, and the part of the ileum (15 cm from cecum) including the inoculation site was collected. After washing the collected part of the ileum, the blocks of PPs were embedded in the OCT compound (Sakura Finetechnical) for immunofluorescence staining or fixed in ice-cold 3% glutaraldehyde/0.1 M sucrose/PBS (pH 7.4) for transmission electron microscopy and energy-dispersive x-ray spectroscopy.

Histopathological study

Tissue samples were fixed in 10% neutral buffered formalin and were trimmed, embedded in paraffin, sectioned, stained with H&E, and examined by light microscopy.

Immunofluorescence staining

To examine the binding and tissue localizations of TGDK, 5 μm frozen sections derived from rhesus macaques inoculated with FITC-labeled TGDK solution were fixed in cold acetone and blocked with 1% nonfat skim milk in PBS^-. FITC-labeled TGDK was detected using a rabbit anti-FITC Ab (Zymed Laboratories) for signal amplification and a tetramethylrhodamine isothiocyanate (TRITC)-labeled anti-rabbit IgG Ab or an Alexa488-labeled anti-rabbit IgG Ab as a secondary Ab. To further examine how TGDK is incorporated into the lymphoid organ, the sections were stained with a PE-labeled anti-CD20 Ab (BD Biosciences) or an anti-CD54 Ab (R&D Systems) labeled with Alexa555 using a Zenon mouse IgG labeling kit (Invitrogen).

To investigate whether gp2 was expressed in rhesus PP M cells, the sections were pretreated with 0.1% Triton X-100, which is used to solubilize the mucus, and then stained with an anti-PV Ab (II-MAP-01; Japan Poliomyelitis Research Institute) labeled with Alexa488 using a Zenon mouse IgG labeling kit (Invitrogen Corporation) or a rabbit anti-gp2 Ab (IMGENEX) labeled with Alexa555 using a Zenon rabbit IgG labeling kit (Invitrogen). To further examine how FITC-labeled TGDK specifically binds to PP M cells, the sections were also pretreated with 0.1% Triton X-100 and then stained with a rabbit anti-FITC Ab and Alexa488-labeled anti-rabbit IgG Ab as a secondary Ab or a rabbit anti-gp2 Ab (IMGENEX) labeled with Alexa555 using a Zenon rabbit IgG labeling kit (Invitrogen). Some sections were counterstained with 4′,6-diamidino-2 phenylindole (DAPI) to show nuclei.

After the staining, slides were washed and analyzed with a Keyence Biozero BZ-8000 (Keyence) and a Flowview FV3000 (Olympus).

Transmission electron microscopy (TEM) and energy-dispersive x-ray spectroscopy (EDS)

Tissue samples were rinsed in PBS with 0.1 M sucrose (pH 7.4) and post-fixed with 1% osmium tetroxide in 0.1 M phosphate buffer at 4°C for 2 h. All the samples were rinsed briefly with 50:50, 70:30, 80:20, 90:10, and 95:5 ethanol/water mixtures and 100% ethanol for 10 min each and three times with 100% ethanol for dehydration, and then embedded in epoxy resin (Quatol 812). One-micrometer sections were cut using a glass knife and then stained with toluidine blue. Suitable areas for ultrastructural study were chosen after examining 1-μm sections under a light microscope. Sections of 60–90 nm were cut on a Leica EM UC6 ultramicrotome using a diamond knife, and sections were mounted on a copper grid and stained with 1% uranyl acetate and Reynolds lead citrate. The grids were examined under a JEOL JEM 1200-EX electron microscope. Furthermore, EDS, which was consigned to JEOL Datum, was performed to quantify TGDK by measuring gold concentration within a specimen.

Preparation of TGDK-conjugated multiantigens

To examine the in vivo effect of TGDK on M cell targeting, TGDK was conjugated via a Hubantigen with rhesus CCR5-derived cyclopeptide (rcDDR5) and BSA. To prepare a Hubantigen, an eight-arm functional polyethylene glycol (PEG) with *p*-nitrophenyl groups, SUNBRIGHT HGEO-200NP (NOF Corporation; 1 equivalent), was mixed with an eight-arm functional PEG with primary amino groups, SUNBRIGHT HGEO-200PA (NOF; 7.2 equivalent), in DMF for 16 h. The resulting Hubantigen was dialyzed in Spectrapore dialysis bags (Spectrum Laboratories; molecular weight cut off = 12–14 kDa) against Milli-Q water for 2 days. The dialysate was lyophilized and used as a Hubantigen. To prepare rcDDR5, a rhesus CCR5-derived linear dodecapeptide (H_2N-KRSQREGLHYTG-COOH), in which all side-chain groups are protected, was synthesized using an automatic peptide synthesizer, and cyclized, as previously described (28). To bind both TGDK and rcDDR5 to the Hubantigen, the amino group of ethylenediamine in TGDK (two equivalents) or of Lys^1 in the deprotected rcDDR5 (two equivalents) was conjugated to four-armed functional PEG, SUNBRIGHT PTE-100NP (NOF; 1 equivalent). Finally, the Hubantigen (168 mg) was coupled to the four-armed PEG-ylated TGDK (12 μmol) and -rcDDR5 (12 μmol) in DMF for 24 h and then covalently bound to BSA for 6 h. The TGDK-conjugated Ag was dialyzed for 15 h against PBS^-, and the dialysate was lyophilized with lactose. The resulting Ag was encapsulated in enteric-coated capsules and included TGDK (56 nmol/capsule), rcDDR5 (90 nmol/capsule), lactose (146 μmol/capsule), and BSA (4.5 nmol/capsule). In contrast, a control Ag also included BSA (4.5 nmol/capsule), but it was not conjugated via a covalent

bond with a Hubantigen. Furthermore, the control Ag did not include TGDK and rcDDR5.

Immunization schedule

All of the rhesus macaques were housed in individual cages and maintained in accordance with the rules and guidelines of the National Institute for Infectious Diseases for experimental animal welfare. Five 4- to 6-year-old rhesus macaques (no. 6–10) were orally administered with two enteric-coated capsules containing TGDK-conjugated multiantigens at 0, 2, and 6 wk. Another five rhesus macaques (no. 1–5) were immunized with an enteric-coated capsule including control Ag following the same immunization schedule as that for the controls. Stool samples were obtained at 0, 12, 13, and 14 wk postinitial immunization (wpim), which were then subjected to anti-BSA Ab ELISA and rcDDR5-coupled multipin ELISA in accordance with the method of Misumi et al. (29).

Sample collection and processing

Acetone powder was prepared by adding fecal pellets (3 g) with stirring to 3 ml of cold acetone. The powder was then washed three times with cold ether and dried until no trace of ether remained. The acetone powder (100 mg) was resuspended in 400 μl of 1% MPC polymer solution (NOF) and incubated at 37°C for 30 min, and then on ice for 1 h. The suspensions were centrifuged at 13,000 × *g* for 5 min to remove fecal solids. The processed fecal Ab samples were subjected to anti-BSA Ab ELISA and rcDDR5-coupled multipin ELISA.

Anti-BSA Ab ELISA

Abs against BSA in stool samples were detected by ELISA. For evaluation of stool Abs, each well of a flat-bottom 96-well maxisorp microplate (Nunc) was coated with 50 μl of coating buffer (pH 8.0) containing BSA (100 μg/ml) and incubated at room temperature (RT) overnight. The wells were washed with 150 μl of Milli-Q water with 0.1% Tween 80 with complete decanting and rinsed with Milli-Q water. Subsequently, 100 μl of blocking buffer, composed of 1% skim milk in Milli-Q water, was added to each well and incubated for 2 h at RT to occupy all unbound sites. Washing was repeated, as described above, followed by the addition of 50 μl of a fecal Ab sample diluted 1/10 in PBS^- to each well. Plates were incubated for 2 h at RT and then washed with 0.1% Tween 80, and 50 μl of peroxidase-conjugated goat anti-monkey IgA (diluted 1/5000) was added to each well and incubated for 1 h at RT before the plate was washed. Fifty microliters 3,3′,5,5′-tetramethylbenzidine solution (Wako Pure Chemical) as the substrate was added to each well and incubated at room temperature. Absorbance was measured at 450/630 nm using a microplate reader.

rcDDR5-coupled multipin ELISA

A rhesus CCR5-derived linear dodecapeptide (H_2N-ERSQREGLHYTG-COOH) in which all side-chain groups are protected was synthesized using an automatic peptide synthesizer and was cyclized by bond formation between the α-carboxyl group of Gly and the α-amino group of Glu after removal of the resin. The γ-carboxyl group of Glu in the protected cyclic dodecapeptide was conjugated to MultiPin block (Mimotopes). The block was used for detecting anti-CCR5 Abs in stool samples in accordance with the method of Misumi et al. (28).

Determination of total number of SIV DNA copies

The total number of SIVmac239 DNA copies was determined to monitor SIV infection and estimate the neutralizing activity of antisera. The relative change in the number of SIV DNA copies indicates the degree of neutralizing activity. Percentage of copies in HSC-F infected with SIVmac239 in the presence of a 14-wpim stool sample is expressed relative to that in the presence of a 0-wpim stool sample, which is considered 100%. HSC-F cells (4×10^6) were infected with SIVmac239 (50 ng, measured using p27 Ag) in the presence of the 0- and 14-wpim stool samples, dialyzed (cutoff, 100 kDa) against PBS^-, and diluted in PBS^-. The inhibitory effect of the stool sample was investigated at 55-fold final dilution. After 48 h, HSC-F cells were harvested. The total viral DNA obtained after the purification procedure (29) was used for SYBR Green real-time PCR assay, as previously described (30), with some modifications. Briefly, primers that recognize specific and highly conserved sequences on the *gag* region of SIV described by Ui et al. (31) were selected. The sequences of SIV *gag* primers were 5′-GGAAATTACCCAGTACAACAAATAGG-3′ and 5′-TC TATCAATTTTACCCAGGCATTTA-3′. The SIV *gag* gene was amplified in 20 μl of a PCR mixture consisting of 10 μl of 2× master mix containing modified DyNAmo hot start DNA polymerase, SYBR Green I, optimized PCR buffer, 5 mM $MgCl_2$, a dNTP mix including dUTP (Finnzymes), 2 μl of each primer, and 8 μl of cDNA. PCR was conducted as follows: initial activation of hot start DNA polymerase at 95°C for 15 min; 40 cycles of four steps of 95°C for 10 s, 57°C for 20 s, 72°C for 20 s, and 76°C for 2 s. At the end of the amplification cycle, melting temperature analysis was conducted by gradually increasing temperature (0.5°C/s) to 95°C. Amplification, data acquisition, and analysis were conducted with the DNA Engine Opticon 2 System (Bio-Rad) using Opticon Monitor version 3.0 software.

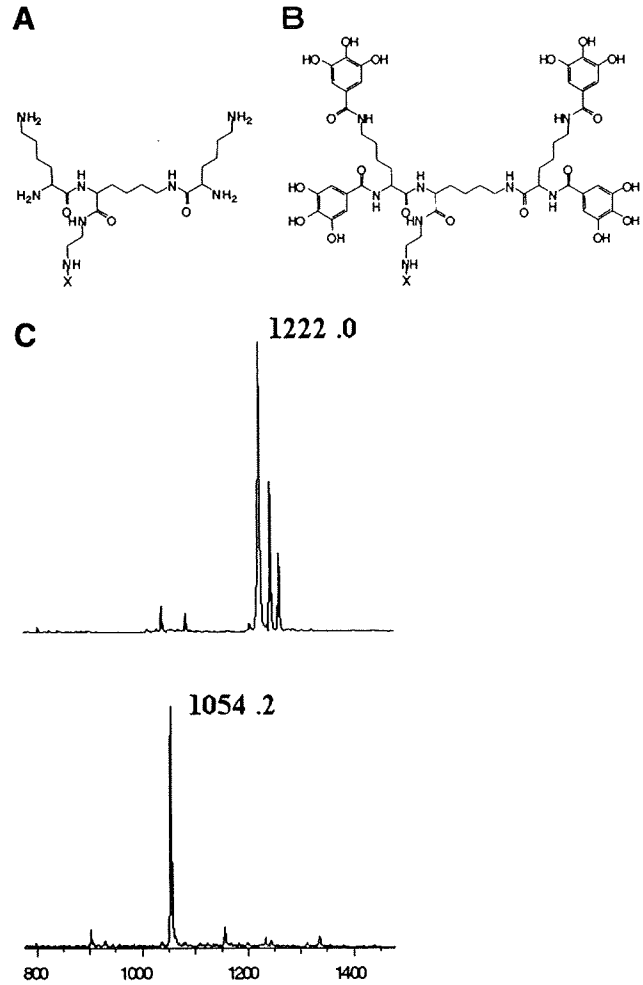

FIGURE 1. Structure and mass spectrometry of TGDK. *A*, D-lysine dendrimer. *B*, TGDK. *C*, MALDI-TOF mass spectrometry spectrum of intermediate compound, (3,4,5-trimethoxybenzoyl)$_4$-D-lyseine dendrimer, and TGDK. The spectra exhibited two peaks at m/z 1222.0 and 1054.2: the *upper peak* is that of the ion derived from the reaction intermediate, (3,4,5-trimethoxybenzoyl)$_4$-D-lyseine dendrimer, and the *lower peak* is that of the ion derived from TGDK.

In vitro human M cell model

The human M cell model was constructed using cocultures of Caco-2 cells and Raji cells in accordance with the method of Kernéis et al. (32) with slight modification. We seeded Caco-2 cells by adding 1×10^6 cells on the lower face of 3-μm-pore Transwell filters and culturing them overnight. The filters were then transferred to the Transwell device with the epithelial cells facing the lower chamber of the cluster plates. Caco-2 cells were cultured until they were fully differentiated (21 days). Raji B cells (10^6) were added to the upper chamber facing the basolateral side of Caco-2 cells. The cultures were maintained for 3 days. Caco-2 cell monolayers were washed with PBS^- and incubated with FITC-labeled TGDK, or FITC-labeled D-lysine dendrimer with or without PV (type II, $10^{4.5}$–$10^{5.5}$ cell culture infective doses 50%) for 30 min. To examine the localization of PV and M cell makers (i.e., gp2, CD54, and integrin β_1), the monolayers were stained with an anti-PV Ab (II-MAP-01; Japan Poliomyelitis Research Institute), an anti-gp2 polyclonal Ab (IMGENEX) labeled with

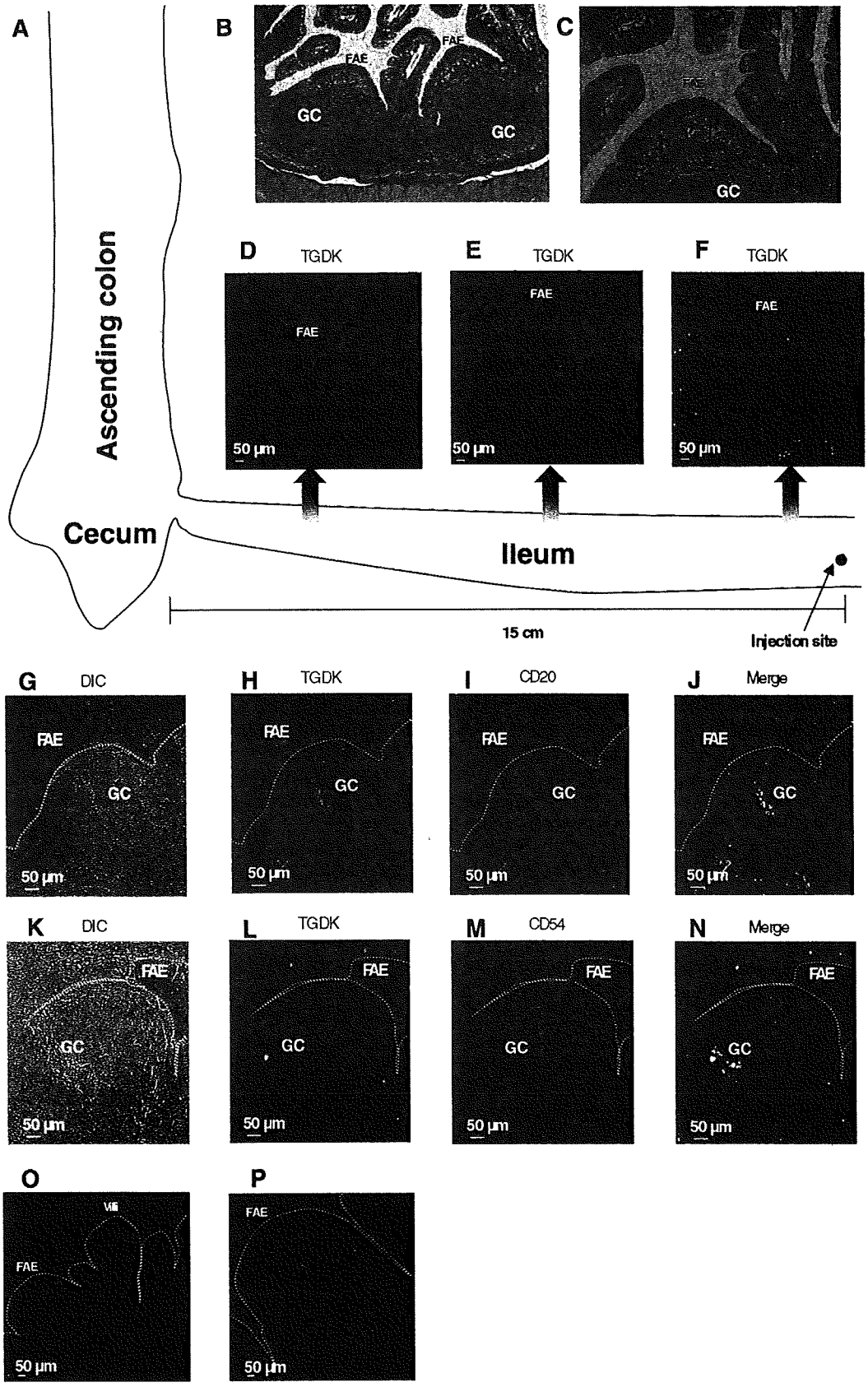

FIGURE 2. Association of TGDK with rhesus PP FAE and accumulation of TGDK within the GCs. *A*, Schematic diagram of rhesus ileum. *B* and *C*, H&E staining of rhesus PPs. *D–F*, FITC-labeled TGDK was inoculated into the lumen of the ileum at 15 cm from the ileocecal valve. One hour after TGDK inoculation, the portion between the injection site of TGDK and the ileocecal valve was excised and subjected to immunofluorescence analysis. Frozen sections of rhesus macaque PPs were labeled with mAbs (anti-CD20 Ab (*I*) and anti-CD54 Ab (*M*); red), and TGDK was stained, as described in *Materials and Methods* (red or green) (*D–F*, *H*, and *L*). Differential interference contrast (DIC) (*G* and *K*), merged (*J* and *N*), and control (*O*, Alexa488-labeled anti-rabbit IgG, or *P*, TRITC-labeled anti-rabbit IgG) images are shown.

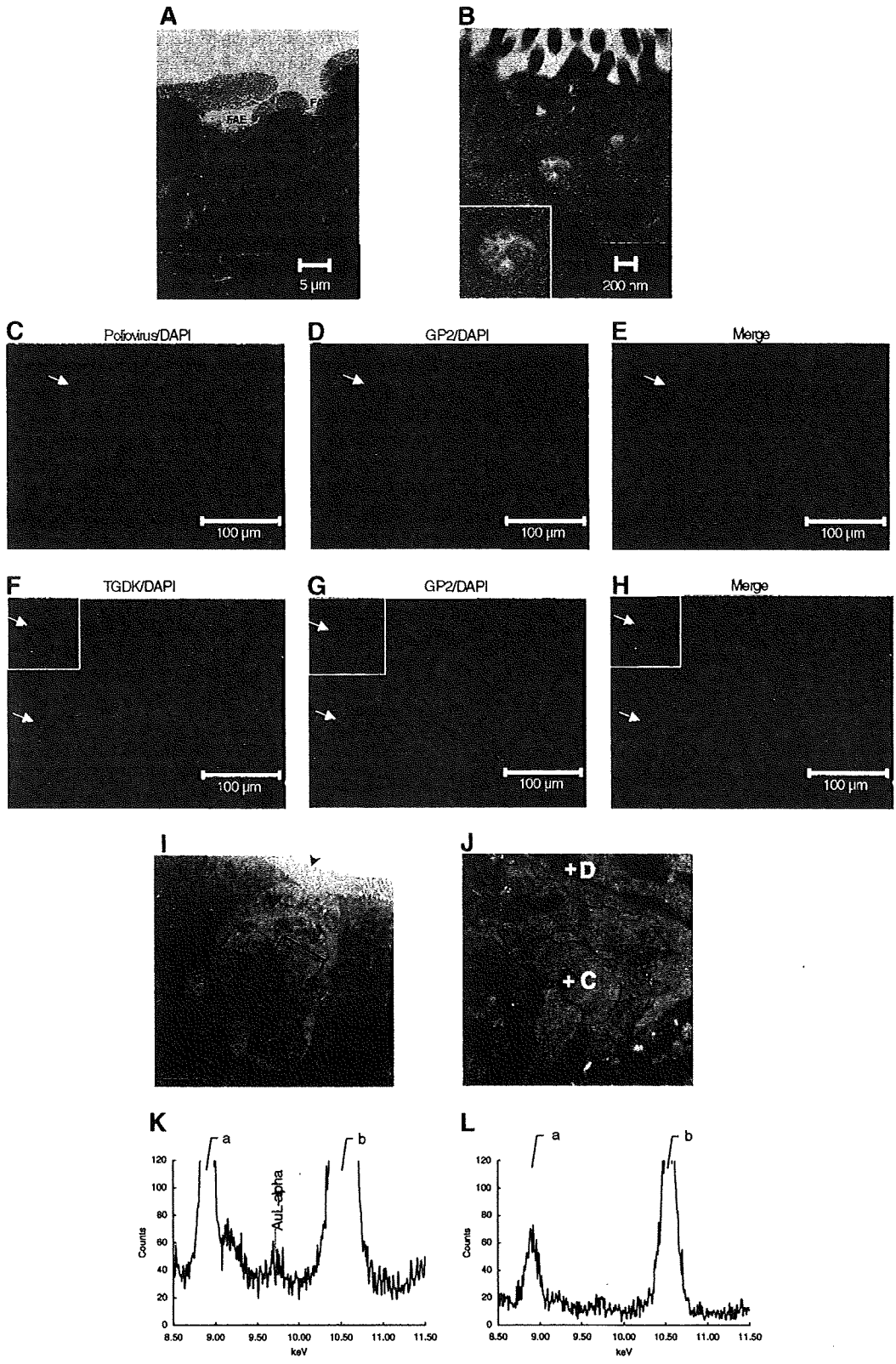

FIGURE 3. TGDK can efficiently penetrate into rhesus PP M cells. PV, FITC-labeled TGDK, or 10-nm gold-labeled TGDK was inoculated into the lumen of the ileum, as described in *Materials and Methods*. After the inoculation, the portion between the inoculation site and the ileocecal valve was excised and subjected to electron microscopies (*A*, *B*, *I*, and *J*), immunofluorescence analysis (*C–H*), or EDS (*K* and *L*). *A*, TEM image of typical M cells in the PP. *B*, TEM image of *B* shown in *A*. *Inset* (the magnified TEM image of dotted square in *B*), PV is transcytosed through rhesus PP M cells. *C–H*, Frozen sections of rhesus macaque PPs were labeled with mAbs (anti-PV Ab (*C*) and anti-gp2 Ab (*D* and *G*)), and TGDK were stained, as described in *Materials and Methods* (*F*). Merged images are shown (*E* and *H*). *I*, TEM view of rhesus PP M cells, which had short (arrowhead) and irregular microvilli and pocket structures containing lymphocytes (indicated by *L*). *J*, Depicts a higher-magnification image of *I*. *K* and *L*, Graphs show EDS of *spots C* and *D* in *J*, confirming the presence of gold-labeled TGDK. The *a* signals come from Cu (8.904 keV), which is attributed to the sample holder, and the *b* signal contains the signal of OsLβ (10.354 keV).

Alexa555 using a Zenon mouse IgG labeling kit (Invitrogen), a mouse anti-human CD54 Ab (R&D Systems), or a mouse anti-human integrin $\alpha_5\beta_1$ Ab (Chemicon International), and then incubated with or without TRITC-labeled goat anti-mouse IgG (Jackson ImmunoResearch Laboratories). At the end of the staining, slides were washed and incubated with DAPI for nuclear staining. Finally, the monolayers were washed and analyzed with a Keyence Biozero BZ-8000. To investigate whether TGDK was specifically transported in human M cell model, the assay was conducted in the presence of 100 μM FITC-labeled TGDK or FITC placed in the lower chamber. The monolayers including M cells or Caco-2 control monolayers were incubated for 2 h at 37°C. FITC-labeled TGDK or FITC, transported from the lower chamber to the upper chamber, was quantified using a CORONA Multi Microplate Reader.

Results

Synthesis of TGDK

UEA-1, an α-L-fucose-specific lectin, has been of particular interest owing to its M cell specificity in the mouse model and its applicability to proof-of-concept studies of vaccine delivery to APCs (33). However, lectins are susceptible to proteolytic degradation in the gastrointestinal tract, and their cytotoxic effects also limit their use as targeting agents to deliver vaccines to M cells. One approach to overcoming these limitations is to synthesize small organic molecules that are able to mimic the function of lectins. Lambkin et al. (26, 34) reported that a synthetic multivalent polygalloyl derivative (SMPD) is a competitor of UEA-1 and appears to have high affinity for the fucose receptor on murine M cells. Its advantages include its stability and suitability for incorporation into delivery systems using routine chemical procedures. In this study, we also chose a versatile scaffold with branched D-lysine (Fig. 1*A*). An aminoethyl group was introduced into the lysine dendrimeric scaffold to allow its linkage with a candidate immunogen. Furthermore, gallic acid was selected as a polyphenolic functional group and coupled with α- and ε-amino groups of lysine residues in the lysine dendrimer (Fig. 1*B*). As shown in Fig. 1*C*, the spectra of purified $(3,4,5\text{-trimethoxybenzoyl})_4$-D-lysine dendrimer and TGDK exhibited major peaks at m/z 1222.0 (Fig. 1*C*, *upper spectrum*) and 1054.2 (Fig. 1*C*, *lower spectrum*), respectively. The difference in molecular mass indicates the complete deprotection of the methyl group by boron tribromide.

TGDK transport through follicle-associated epithelium (FAE) of rhesus macaque PPs

To examine whether TGDK was effectively transported through FAE of PPs in vivo, FITC-labeled TGDK was inoculated into the rhesus macaque ileum (Fig. 2*A*). One hour after the injection, the tissue was subjected to immunofluorescence analysis. As shown in Fig. 2, *B* and *C*, the large PP is found in the lumen of the terminal ileum in rhesus macaques. Light microscopy revealed the typical structure of a mucosal lymphoid follicle, composed of germinal centers (GCs) and a dome area bulging into the lumen (Fig. 2, *B* and *C*). The closer the section to the injection site, the larger the amount of TGDK reaching GCs through FAE of PPs (Fig. 2, *D–F*). When PPs from different sections (~7.5 cm from the injection site) were further observed, TGDK was clearly detected in the GCs of PPs (Fig. 2, *H* and *L*). GC cells can be stained with anti-CD20 and anti-CD54 Abs, the staining patterns reflecting reactivity with B cell lymphocytes and the follicular dendritic reticulum in nonhuman primates and humans, respectively (35–37). As shown in Fig. 2, *I* and *M*, CD20 and CD54 were expressed within the GCs of rhesus macaques. Fig. 2, *J* and *N*, shows the patterns of double fluorostaining for TGDK/CD20 or TGDK/CD54 in the GCs of PPs. These results indicate that TGDK efficiently enters into GCs through FAE of PPs in rhesus macaques.

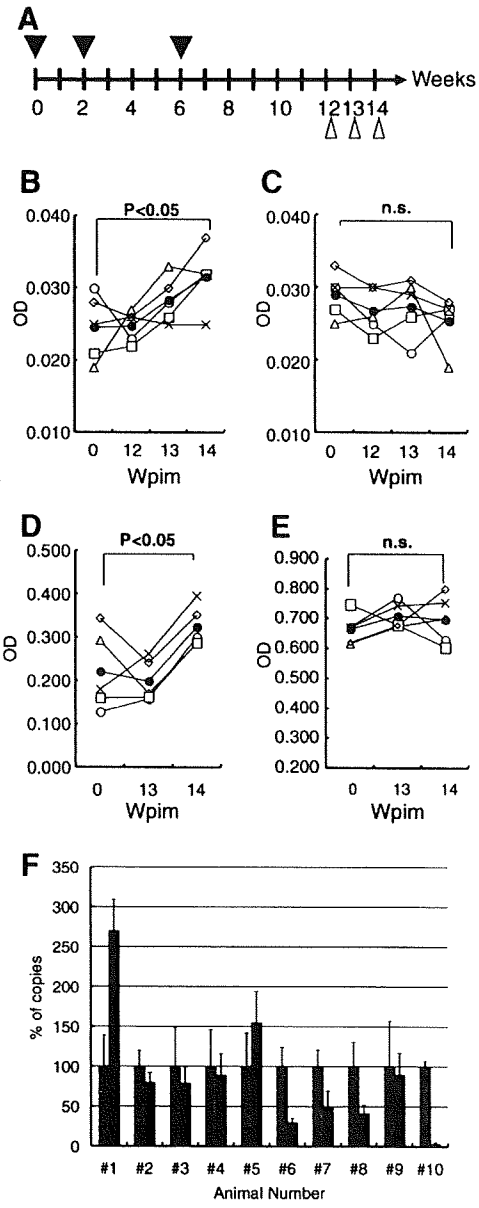

FIGURE 4. Oral immunization schedule and detection of anti-BSA or anti-rcDDR5 Abs in rhesus macaques. *A*, Immunization schedule for rhesus macaques. Five rhesus macaques (no. 6–10) were orally immunized at 0, 2, and 6 wk with TGDK-conjugated multiantigens. Another five macaques (no. 1–5) were immunized with the control Ag. Stool sampling was performed at 12, 13, and 14 wpim. Stool samples (1/10 dilution) obtained after immunization with TGDK-conjugated multiantigen (*B*; macaque no. 6 (○), 7 (△), 8 (■), 9 (◇), and 10 (×)) or control Ag (*C*; macaque no. 1 (○), 2 (△), 3 (■), 4 (◇), and 5(×)) were examined to investigate whether the anti-BSA mucosal IgA (*B* and *C*) or anti-rcDDR5 mucosal IgA (*D* and *E*) can be raised in rhesus macaques by anti-BSA ELISA and the rcDDR5-coupled multipin ELISA, as described in *Materials and Methods*. ○, Show the average OD values. *F*, Furthermore, the inhibitory effect of the stool samples from vaccinated (no. 6–10) and control groups (no. 1–5) on in vitro SIV infection was also investigated, as described in *Materials and Methods*. Percentage of copies in HSC-F infected with SIVmac239 in the presence of the 14-wpim stool sample (■) is expressed relative to that in the presence of the 0-wpim stool sample (▤), which is considered 100%.

Internalization of TGDK by PP M cells

To investigate whether rhesus macaque PP M cells can specifically take up TGDK, the rhesus macaque ileum was inoculated with FITC-labeled TGDK and subjected to immunofluorescence

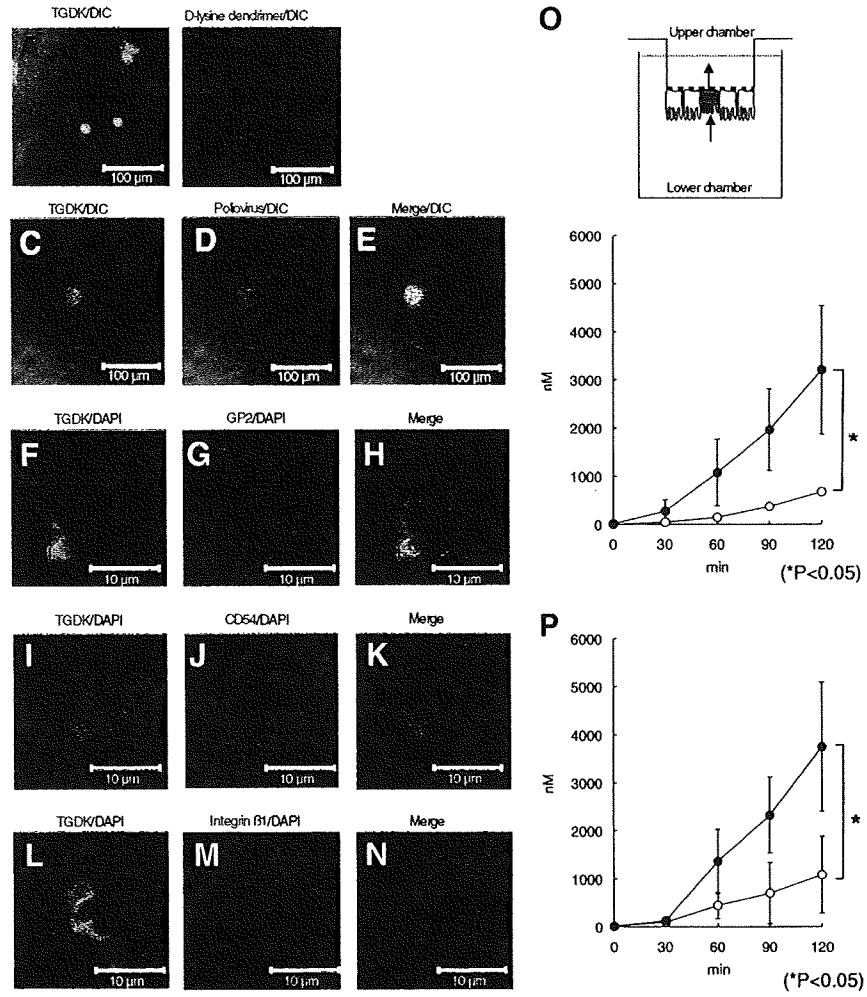

FIGURE 5. Association of TGDK with human M-like cells and transcytosis of TGDK. The Caco-2/Raji B monolayer was stained with FITC-labeled TGDK (*A*, *C*, *F*, *I*, and *L*, green) or the FITC-labeled D-lysine dendrimer (*B*, green), as described in *Materials and Methods*. Because it is known that PV can bind to M-like cells, the Caco-2/Raji B monolayer was labeled with an anti-PV Ab (*D*, red). The monolayer was further labeled with mAbs (anti-gp2 (*G*), anti-CD54 (*J*), and anti-integrin β_1 Abs (*M*), red). *A* and *C*, Show the merge image of DIC and a fluorescence image of FITC-labeled TGDK. *B*, Shows the merge image of DIC and a fluorescence image of FITC-labeled D-lysine dendrimer. *D*, Shows the merge image of DIC and a fluorescence image of monolayer labeled with an anti-PV Ab. *F*, *I*, and *L*, Show the patterns of double fluorostaining for TGDK/DAPI. *G*, *J*, and *M*, Show the patterns of double fluorostaining for gp2/DAPI, CD54/DAPI, and integrin β_1/DAPI. Furthermore, merged (*E*, *H*, *K*, and *N*) images are shown. *O*, To investigate the transcytosis activity of TGDK, the monolayers including M-like cells (●) or Caco-2 control monolayers (○) were incubated with FITC-labeled TGDK. *P*, To investigate the transcytosis efficacy of TGDK, the monolayers including M-like cells were incubated with FITC-labeled TGDK (●) or FITC (○). FITC-labeled TGDK or FITC transported from the lower chamber to the upper chamber was quantified by a CORONA Multi Microplate Reader.

analysis (Fig. 3). Recently, Terahara et al. (38) reported that gp2 is specifically expressed at a high level in mouse PP M cells. However, the expression of gp2 in rhesus PP M cells remains to be clarified in rhesus macaque. Sicinski et al. (39) reported that PV is found specifically adhering to the surface projections of M cells and in vesicles in M cells. Fig. 3*A* shows a typical TEM image of PP M cells. As expected, PV was transcytosed through typical intestinal rhesus PP M cells (Fig. 3*B*). Therefore, we confirmed whether gp2 was expressed in rhesus PP M cells, in which PV was transcytosed. Immunofluorescence analysis demonstrated that gp2 was expressed in rhesus PP M cells (Fig. 3*D*), which were recognized by the anti-PV Ab (Fig. 3*C*). These results indicated that gp2 was expressed in rhesus PP M cells. To further investigate whether TGDK specifically binds to PP M cells, the localization of TGDK was confirmed by counterstaining with the anti-gp2 Ab. As shown in Fig. 3, *F* and *G*, TGDK was colocalized with gp2. These results indicated that TGDK specifically binds to rhesus M cells.

To investigate whether TGDK is transcytosed through PP M cells, the rhesus macaque ileum was inoculated with gold-labeled TGDK and subjected to EDS (Fig. 3). The advantage of EDS is that gold-labeled TGDK can be directly detected when TGDK is completely embedded in an ultrathin section. The characteristic x-ray peak from gold (AuL-α: ~9.712 keV) is used to confirm the presence of nano-gold particles in the cytoplasm of a PP M cell within a section (Fig. 3*I*). EDS demonstrated the presence of gold-labeled TGDK in the cytoplasm of a PP M cell (*spot C*; Fig. 3, *J* and *K*), but not in the cytoplasm of a lymphocyte within a PP M cell (*spot D*; Fig. 3, *J* and *L*). In contrast, gold-labeled TGDK was not detected in intestinal epithelial cells in FAE of PPs. Taken together, these results indicate that inoculation of TGDK into the rhesus macaque ileum containing PPs shows the clear targeting of M cells and transcytosis of TGDK, and rhesus macaque PP M cells have the ability to take up TGDK from the lumen.

Immunization of rhesus macaques with TGDK-conjugated multiantigens and induction of BSA- and rcDDR5-specific Abs

To examine the in vivo effect of TGDK on M cell targeting in nonhuman primates, five rhesus macaques were immunized with TGDK-conjugated multiantigens containing BSA and rcDDR5 by oral administration according to the time schedule shown in Fig. 4*A*. Another five rhesus macaques were immunized with the control Ag. Although BSA-specific IgA in stool samples was significantly induced in the group immunized with TGDK-conjugated multiantigens at 14 wpim (Fig. 4*B*; $p < 0.05$ in repeated measures ANOVA), the immunization with the TGDK-conjugated multiantigen unfortunately induced only weak anti-BSA Ab responses. The result suggests that the induction of a stronger anti-BSA Ab response may be required for a higher content of BSA in the TGDK-conjugated multiantigen. In contrast, the immunization of rhesus macaques with the control Ag did not induce BSA-specific IgA in stool samples (Fig. 4*C*).

Our previous studies demonstrated that the rhesus macaque antisera raised against cDDR5 mimicking the conformation-specific domain of human CCR5 reacted with both human and macaque CCR5s, and potently suppressed infection by the R5 HIV-1 laboratory isolate (HIV_{JRFL}), R5 HIV-1 primary isolates (clade

A:$HIV_{93RW004}$ and clade C:HIV_{MJ4}), and a pathogenic $SHIV_{SF162P3}$ bulk isolate in vitro (29). In addition, our recent data demonstrate that mouse anti-rcDDR5-specific IgG can inhibit in vitro SIV infection (40). Therefore, the stool samples from the group immunized with TGDK-conjugated multiantigens were also examined by rcDDR5-coupled multipin ELISA to determine whether rcDDR5-specific mucosal IgA was induced. As shown in Fig. 4*D*, rcDDR5-specific IgA in stool samples was significantly induced in the group immunized with TGDK-conjugated multiantigens. In contrast, the immunization of rhesus macaques with the control Ag did not induce rcDDR5-specific IgA in stool samples (Fig. 4*E*). Although we investigated whether rcDDR5-specific mucosal IgM or IgG was also induced, the rcDDR5-specific IgM or IgG in stool samples was not significantly induced (data not shown). To further assess neutralizing activity, we performed an in vitro neutralization assay using SIVmac239. Interestingly, neutralizing activity tended to increase with the titer of the anti-rcDDR5 IgA in stool samples (Fig. 4*F*). These data suggest that TGDK-mediated vaccine delivery system represents a potential approach to develop M cell-targeted mucosal vaccines.

Selective binding and transcytosis of TGDK in human in vitro M cell model

Although TGDK promises to be an M cell targeting molecule in nonhuman primates, it still remains unclear whether TGDK effectively targets human M cells. Kernéis et al. (32) developed an in vitro human M cell model that is useful for facilitating the design of oral vaccines and efficient mucosal drug delivery systems. Therefore, we evaluated whether TGDK selectively binds to human M-like cells and is capable of transcytosis. As shown in Fig. 5, *A* and *B*, the spotlike staining of the apical surface of epithelial cells in the model with the FITC-labeled TGDK was observed, but hardly in the model with the FITC-labeled D-lysine dendrimer. Because Sicinski et al. (39) demonstrated that PV enters the human host through intestinal M cells, we examined whether TGDK can colocalize with PV on the apical surface of the model (Fig. 5, *C—E*). Immunofluorescence analysis demonstrated that M cells in the model showed costaining of TGDK and PV. Furthermore, because human M cells express gp2, CD54, and $\alpha_5\beta_1$ integrin on their surface, the apical surface of epithelial cells in the model was also stained with the anti-gp2, anti-CD54, or anti-$\alpha_5\beta_1$ integrin Ab (Fig. 5, *G*, *J*, and *M*) (41–43). Fig. 5, *G*, *J*, and *M*, shows that gp2, CD54, and $\alpha_5\beta_1$ integrin are expressed on the apical surface. Fig. 5, *H*, *K*, and *N*, shows the patterns of triple fluorostaining for TGDK/gp2/DAPI, TGDK/CD54/DAPI, or TGDK/$\alpha_5\beta_1$ integrin/DAPI in this model.

Transcytotic activity was also monitored for 120 min at 37°C. TGDK was effectively transported at 37°C through the monolayers containing M cells, but not through control monolayers (Fig. 5*O*; $p < 0.05$ in Mann-Whitney *U* test). To further confirm TGDK-mediated Ag transport, we investigated whether FITC-labeled TGDK is more efficiently transported than FITC, which is postulated as an Ag. As shown in Fig. 5*P*, FITC-labeled TGDK is more efficiently transported than FITC ($p < 0.05$ in Mann-Whitney *U* test). These results indicate that TGDK can significantly bind to human M cells and is capable of transcytosis through M cells in inductive sites, such as PPs.

Discussion

The sexual route is the most important route of HIV transmission in heterosexuals, in which the genital tract provides the virus access to lymphoid cells. In the majority of patients, the initial acquisition of HIV involves passage of the virus across a mucosal surface. Thus, blocking HIV mucosal transmission is key to prevent HIV infection.

Some studies demonstrated that mucosal Ab responses may contribute to the apparent resistance to HIV-1 infection. The studies, in which humoral and cellular responses against HIV-1 in the vaginal secretions of women who remain uninfected despite frequent unprotected sex with HIV-1-infected partners were analyzed, indicated the presence of mucosal IgA Abs to HIV-1 (44–46). Furthermore, the second type of natural resistance is found in persons with CCR5-specific mucosal autoantibodies (47). To attempt to reproduce some of the functional aspects of this natural resistance to HIV infection, many researchers have examined various types of mucosal vaccine candidate against SIV/SHIV infection because they are capable of inducing not only the immunity at the mucosal sites of transmission, which prevents the virus from gaining entry into immune cells, but also the immunity in the systemic circulation.

Could CCR5 be an attractive target for the development of mucosal vaccines? Persons with the homozygous δ32 CCR5 mutation, a 32-bp deletion of the CCR5 gene that results in a lack of cell surface expression of CCR5, have strongly reduced susceptibility to CCR5-dependent HIV-1 infection (48–50). Furthermore, Pastori et al. (51) reported that long-lasting CCR5 internalization by anti-CCR5 Abs in a subset of long-term nonprogressors is associated with a possible protective effect against disease progression, suggesting that induction of anti-CCR5 Abs by a vaccine can reproduce the immune status in long-term nonprogressors. Our previous study demonstrated that the high induction of the anti-CCR5 Ab can suppress viral propagation during acute HIV-1 i.v. transmission in cynomolgus macaques i.p. and s.c. immunized with cDDR5 mimicking the conformation-specific domain of human CCR5 (29). In this study, rcDDR5 was synthesized to induce more specific anti-rhesus CCR5 Abs. Our recent study demonstrates that the immunization of rcDDR5-conjugated KLH induces mouse anti-rcDDR5-specific IgG that specifically binds to rhesus CCR5 and inhibits in vitro SIV infection (40). These observations suggest that CCR5 can be an attractive target for the development of mucosal vaccines. Hence, to reproduce the functional aspects found in long-term nonprogressors with CCR5-specific mucosal autoantibodies, we sought new types of vaccine delivery system for the effective delivery of rcDDR5 to mucosa-associated lymphoid tissues such as PPs, the inductive site for the induction of the Ag-specific immune response.

Lectins have been investigated for targeted Ag delivery to mucosa-associated lymphoid tissues. UEA-1 and *Aleuria aurantia* lectin have high specificity for the carbohydrate moiety α-L-fucose located on the apical membranes of mouse M cells (19, 21, 52). There have been successful efforts made in in vivo targeting in mouse M cells by conjugating UEA-1 to polymerized liposomes (33) and latex particles (53), or by coating poly(D, L-lactide-co-glycolide) particles with the *A. aurantia* lectin (52). However, lectins are of limited value in vaccine delivery owing to their toxicity to humans or sensitivity to intestinal degradation. To overcome these limitations, SMPDs that appear to have high affinity for the fucose receptor on murine M cells were identified from a high-throughput screening of mixture-based compound libraries in a competitive UEA-1-binding assay (26). Although SMPDs may have the potential in oral vaccine targeting in mouse model, it remained unclear whether SMPDs effectively target nonhuman and human M cells.

The macaque model serves several important purposes in current HIV vaccine research. It allows analysis of vaccine safety and proof of immunogenicity in a species more closely related to humans. Furthermore, there are a few interesting options for testing

the effect of a vaccine on a mucosal pathogenic challenge system, such as SIV or SHIV challenges. Therefore, we investigated the M cell targeting potential of a tetragalloyl derivative, TGDK, in an in vivo nonhuman primate model. Our findings suggest that TGDK can serve as a useful targeting molecule for nonhuman primate M cells (Fig. 3). Interestingly, TGDK accumulated in GCs after it transcytosed through M cells from the gut lumen (Fig. 2, *D–F*). Although the mechanism underlying the behavior of TGDK in PP still remains to be elucidated, the ability of TGDK to accumulate in GCs may increase the possibility of interaction of an immunogen, in the form of an immune complex trapped on follicular dendritic cells, with GC B cells.

To assess the efficiency of TGDK as a mucosal delivery system, it is important to examine whether rcDDR5-specific Abs in mucosal secretions are induced in nonhuman primate models. It is generally difficult to induce a long-lasting anti-CCR5 Ab response because CCR5 is continuously exposed to the immune system. Our previous study showed that immunization with cDDR5-MAP induces anti-CCR5 serum production for ~15 wk after the third immunization, although the titer of anti-CCR5 sera declined over time until 21 wpim (29), suggesting that cDDR5-MAP is not suitable as a model Ag for the estimation of TGDK owing to its weak immunogenicity. Therefore, we introduced BSA as a standard model Ag into TGDK-conjugated multiantigens with rcDDR5 via the Hubantigen to estimate the efficiency of TGDK. Furthermore, our recent data indicate that anti-rcDDR5 serum is produced for more than 56 wk when rhesus macaques were inguinally immunized with the TGDK-conjugated multiantigens containing rcDDR5 and BSA without a specific adjuvant (our unpublished data), suggesting that the immunogenicity of TGDK-conjugated multiantigens used to evaluate the effect of TGDK was improved. Five animals were orally immunized with the TGDK-conjugated multiantigen (vaccinated group), and another five were immunized with the Hubantigen and BSA only (control group). Although the immunization with the TGDK-conjugated multiantigen induced only weak anti-BSA Ab responses in the vaccinated group (Fig. 4*B*; $p < 0.05$), rcDDR5-specific IgA in stool samples was significantly induced in the vaccinated group, as shown in Fig. 4*D*. Furthermore, the neutralizing activity tended to increase with the titer of the anti-rcDDR5 Ab in the stool samples (Fig. 4*F*). Taken together, these results show that TGDK is useful for inducing rcDDR5-specific mucosal IgA responses with neutralizing activity, although it is necessary to re-examine the dose of the orally administered TGDK-conjugated multiantigens for the perfect reproduction of the functional aspects found in long-term nonprogressors with CCR5-specific mucosal autoantibodies.

Finally, we examined whether TGDK can be available for human use using the human in vitro M cell model. Giannasca et al. (54) reported that the UEA-1 receptor is not expressed in human PPs, whereas Sharma et al. (55) reported that the UEA-1 binding was observed in M cells of human FAE. Because it further remained unclear whether the binding receptor of UEA-1 is completely the same as that of TGDK, we examined whether TGDK was directly capable of binding to human M-like cells. As shown in Fig. 5, TGDK can specifically bind to human M-like cells and transcytose through M-like cells. These results suggest that the TGDK-mediated vaccine delivery system can be available for mucosal vaccine delivery in humans.

Acknowledgments

We thank Dr. H. Matsunaga (Kumamoto University) for excellent technical assistance in TGDK synthesis. We thank K. Matsuda (Keyence) for excellent technical assistance in immunofluorescence analysis. We thank K. Nozaki, Y. Kudo, H. Kai, and K. Matsuura for excellent technical assistance in in vitro experiments.

Disclosures

The authors have no financial conflict of interest.

References

1. Pope, M., and A. T. Haase. 2003. Transmission, acute HIV-1 infection and the quest for strategies to prevent infection. *Nat. Med.* 9: 847–852.
2. Lackner, A. A., and R. S. Veazey. 2007. Current concepts in AIDS pathogenesis: insights from the SIV/macaque model. *Annu. Rev. Med.* 58: 461–476.
3. Li, Q., L. Duan, J. D. Estes, Z. M. Ma, T. Rourke, Y. Wang, C. Reilly, J. Carlis, C. J. Miller, and A. T. Haase. 2005. Peak SIV replication in resting memory $CD4^+$ T cells depletes gut lamina propria $CD4^+$ T cells. *Nature* 434: 1148–1152.
4. Guadalupe, M., E. Reay, S. Sankaran, T. Prindiville, J. Flamm, A. McNeil, and S. Dandekar. 2003. Severe $CD4^+$ T-cell depletion in gut lymphoid tissue during primary human immunodeficiency virus type 1 infection and substantial delay in restoration following highly active antiretroviral therapy. *J. Virol.* 77: 11708–11717.
5. Mascola, J. R., G. Stiegler, T. C. VanCott, H. Katinger, C. B. Carpenter, C. E. Hanson, H. Beary, D. Hayes, S. S. Frankel, D. L. Birx, and M. G. Lewis. 2000. Protection of macaques against vaginal transmission of a pathogenic HIV-1/SIV chimeric virus by passive infusion of neutralizing antibodies. *Nat. Med.* 6: 207–210.
6. Belyakov, I. M., B. Moss, W. Strober, and J. A. Berzofsky. 1999. Mucosal vaccination overcomes the barrier to recombinant vaccinia immunization caused by preexisting poxvirus immunity. *Proc. Natl. Acad. Sci. USA* 96: 4512–4517.
7. Gherardi, M. M., E. Perez-Jimenez, J. L. Najera, and M. Esteban. 2004. Induction of HIV immunity in the genital tract after intranasal delivery of a MVA vector: enhanced immunogenicity after DNA prime-modified vaccinia virus Ankara boost immunization schedule. *J. Immunol.* 172: 6209–6220.
8. Douce, G., V. Giannelli, M. Pizza, D. Lewis, P. Everest, R. Rappuoli, and G. Dougan. 1999. Genetically detoxified mutants of heat-labile toxin from *Escherichia coli* are able to act as oral adjuvants. *Infect. Immun.* 67: 4400–4406.
9. Belyakov, I. M., S. A. Hammond, J. D. Ahlers, G. M. Glenn, and J. A. Berzofsky. 2004. Transcutaneous immunization induces mucosal CTLs and protective immunity by migration of primed skin dendritic cells. *J. Clin. Invest.* 113: 998–1007.
10. Kang, S. M., Q. Yao, L. Guo, and R. W. Compans. 2003. Mucosal immunization with virus-like particles of simian immunodeficiency virus conjugated with cholera toxin subunit B. *J. Virol.* 77: 9823–9830.
11. Guo, L., X. Lu, S. M. Kang, C. Chen, R. W. Compans, and Q. Yao. 2003. Enhancement of mucosal immune responses by chimeric influenza HA/SHIV virus-like particles. *Virology* 313: 502–513.
12. Sakaue, G., T. Hiroi, Y. Nakagawa, K. Someya, K. Iwatani, Y. Sawa, H. Takahashi, M. Honda, J. Kunisawa, and H. Kiyono. 2003. HIV mucosal vaccine: nasal immunization with gp160-encapsulated hemagglutinating virus of Japan-liposome induces antigen-specific CTLs and neutralizing antibody responses. *J. Immunol.* 170: 495–502.
13. Wang, X., D. M. Hone, A. Haddad, M. T. Shata, and D. W. Pascual. 2003. M cell DNA vaccination for CTL immunity to HIV. *J. Immunol.* 171: 4717–4725.
14. Holmgren, J., C. Czerkinsky, K. Eriksson, and A. Mharandi. 2003. Mucosal immunization and adjuvants: a brief overview of recent advances and challenges. *Vaccine* 21(Suppl. 2): S89–S95.
15. Kraehenbuhl, J. P., and M. R. Neutra. 2000. Epithelial M cells: differentiation and function. *Annu. Rev. Cell. Dev. Biol.* 16: 301–332.
16. Jepson, M. A., M. A. Clark, N. Foster, C. M. Mason, M. K. Bennett, N. L. Simmons, and B. H. Hirst. 1996. Targeting to intestinal M cells. *J. Anat.* 189: 507–516.
17. Clark, M. A., M. A. Jepson, and B. H. Hirst. 1995. Lectin binding defines and differentiates M-cells in mouse small intestine and caecum. *Histochem. Cell Biol.* 104: 161–168.
18. Jepson, M. A., C. M. Mason, M. A. Clark, N. L. Simmons, and B. H. Hirst. 1995. Variations in lectin binding properties of intestinal M cells. *J. Drug Target* 3: 75–77.
19. Clark, M. A., M. A. Jepson, N. L. Simmons, T. A. Booth, and B. H. Hirst. 1993. Differential expression of lectin-binding sites defines mouse intestinal M-cells. *J. Histochem. Cytochem.* 41: 1679–1687.
20. Clark, M. A., M. A. Jepson, N. L. Simmons, and B. H. Hirst. 1995. Selective binding and transcytosis of *Ulex europaeus I* lectin by mouse Peyer's patch M-cells in vivo. *Cell Tissue Res.* 282: 455–461.
21. Giannasca, P. J., K. T. Giannasca, P. Falk, J. I. Gordon, and M. R. Neutra. 1994. Regional differences in glycoconjugates of intestinal M cells in mice: potential targets for mucosal vaccines. *Am. J. Physiol.* 267: G1108–G1121.
22. Gebert, A., and W. Posselt. 1997. Glycoconjugate expression defines the origin and differentiation pathway of intestinal M-cells. *J. Histochem. Cytochem.* 45: 1341–1350.
23. Manocha, M., P. C. Pal, K. T. Chitralekha, B. E. Thomas, V. Tripathi, S. D. Gupta, R. Paranjape, S. Kulkarni, and D. N. Rao. 2005. Enhanced mucosal and systemic immune response with intranasal immunization of mice with HIV peptides entrapped in PLG microparticles in combination with *Ulex europaeus-I* lectin as M cell target. *Vaccine* 23: 5599–5617.
24. Wang, X., I. Kochetkova, A. Haddad, T. Hoyt, D. M. Hone, and D. W. Pascual. 2005. Transgene vaccination using *Ulex europaeus agglutinin I* (UEA-1) for targeted mucosal immunization against HIV-1 envelope. *Vaccine* 23: 3836–3842.

25. Wu, Y., X. Wang, K. L. Csencsits, A. Haddad, N. Walters, and D. W. Pascual. 2001. M cell-targeted DNA vaccination. *Proc. Natl. Acad. Sci. USA* 98: 9318–9323.
26. Lambkin, I., C. Pinilla, C. Hamashin, L. Spindler, S. Russell, A. Schink, R. Moya-Castro, G. Allicotti, L. Higgins, M. Smith, et al. 2003. Toward targeted oral vaccine delivery systems: selection of lectin mimetics from combinatorial libraries. *Pharm. Res.* 20: 1258–1266.
27. Takahashi, Y., S. Misumi, A. Muneoka, M. Masuyama, H. Tokado, K. Fukuzaki, N. Takamune, and S. Shoji. 2008. Nonhuman primate intestinal villous M-like cells: an effective poliovirus entry site. *Biochem. Biophys. Res. Commun.* 368: 501–507.
28. Misumi, S., R. Nakajima, N. Takamune, and S. Shoji. 2001. A cyclic dodecapeptide-multiple-antigen peptide conjugate from the undecapeptidyl arch (from Arg^{168} to Cys^{178}) of extracellular loop 2 in CCR5 as a novel human immunodeficiency virus type 1 vaccine. *J. Virol.* 75: 11614–11620.
29. Misumi, S., D. Nakayama, M. Kusaba, T. Iiboshi, R. Mukai, K. Tachibana, T. Nakasone, M. Umeda, H. Shibata, M. Endo, et al. 2006. Effects of immunization with CCR5-based cycloimmunogen on simian/HIVSF162P3 challenge. *J. Immunol.* 176: 463–471.
30. Gibellini, D., F. Vitone, E. Gori, M. La Placa, and M. C. Re. 2004. Quantitative detection of human immunodeficiency virus type 1 (HIV-1) viral load by SYBR green real-time RT-PCR technique in HIV-1 seropositive patients. *J. Virol. Methods* 115: 183–189.
31. Ui, M., T. Kuwata, T. Igarashi, K. Ibuki, Y. Miyazaki, I. L. Kozyrev, Y. Enose, T. Shimada, H. Uesaka, H. Yamamoto, et al. 1999. Protection of macaques against a SHIV with a homologous HIV-1 Env and a pathogenic SHIV-89.6P with a heterologous Env by vaccination with multiple gene-deleted SHIVs. *Virology* 265: 252–263.
32. Kernéis, S., A. Bogdanova, J. P. Kraehenbuhl, and E. Pringault. 1997. Conversion by Peyer's patch lymphocytes of human enterocytes into M cells that transport bacteria. *Science* 277: 949–952.
33. Clark, M. A., H. Blair, L. Liang, R. N. Brey, D. Brayden, and B. H. Hirst. 2001. Targeting polymerized liposome vaccine carriers to intestinal M cells. *Vaccine* 20: 208–217.
34. Hamashin, C., L. Spindler, S. Russell, A. Schink, I. Lambkin, D. O'Mahony, R. Houghten, and C. Pinilla. 2003. Identification of novel small-molecule *Ulex europaeus I* mimetics for targeted drug delivery. *Bioorg. Med. Chem.* 11: 4991–4997.
35. Veazey, R. S., M. Rosenzweig, D. E. Shvetz, D. R. Pauley, M. DeMaria, L. V. Chalifoux, R. P. Johnson, and A. A. Lackner. 1997. Characterization of gut-associated lymphoid tissue (GALT) of normal rhesus macaques. *Clin. Immunol. Immunopathol.* 82: 230–242.
36. Dustin, M. L., R. Rothlein, A. K. Bhan, C. A. Dinarello, and T. A. Springer. 1986. Induction by IL 1 and interferon-γ: tissue distribution, biochemistry, and function of a natural adherence molecule (ICAM-1). *J. Immunol.* 137: 245–254.
37. Koopman, G., H. K. Parmentier, H. J. Schuurman, W. Newman, C. J. Meijer, and S. T. Pals. 1991. Adhesion of human B cells to follicular dendritic cells involves both the lymphocyte function-associated antigen 1/intercellular adhesion molecule 1 and very late antigen 4/vascular cell adhesion molecule 1 pathways. *J. Exp. Med.* 173: 1297–1304.
38. Terahara, K., M. Yoshida, O. Igarashi, T. Nochi, G. S. Pontes, K. Hase, H. Ohno, S. Kurokawa, M. Mejima, N. Takayama, et al. 2008. Comprehensive gene expression profiling of Peyer's patch M cells, villous M-like cells, and intestinal epithelial cells. *J. Immunol.* 180: 7840–7846.
39. Sicinski, P., J. Rowinski, J. B. Warchol, Z. Jarzabek, W. Gut, B. Szczygiel, K. Bielecki, and G. Koch. 1990. Poliovirus type 1 enters the human host through intestinal M cells. *Gastroenterology* 98: 56–58.
40. Misumi, S., A. Eto, R. Mitsumata, M. Yamada, N. Takamune, and S. Shoji. 2008. Development of cell-expressed and virion-incorporated CCR5-targeted vaccine. *Biochem. Biophys. Res. Commun.* 377: 617–621.
41. Ohno, H., K. Hase, and K. Kawano. 2008. Antigen recognition, uptake and receptor on M cells. *Clin. Immunol. Allergol.* 19: 1–9.
42. Ueki, T., M. Mizuno, T. Uesu, T. Kiso, and T. Tsuji. 1995. Expression of ICAM-I on M cells covering isolated lymphoid follicles of the human colon. *Acta Med. Okayama* 49: 145–151.
43. Gullberg, E., A. V. Keita, S. Y. Salim, M. Andersson, K. D. Caldwell, J. D. Soderholm, and P. Artursson. 2006. Identification of cell adhesion molecules in the human follicle-associated epithelium that improve nanoparticle uptake into the Peyer's patches. *J. Pharmacol. Exp. Ther.* 319: 632–639.
44. Beyrer, C., A. W. Artenstein, S. Rugpao, H. Stephens, T. C. VanCott, M. L. Robb, M. Rinkaew, D. L. Birx, C. Khamboonruang, P. A. Zimmerman, et al. 1999. Epidemiologic and biologic characterization of a cohort of human immunodeficiency virus type 1 highly exposed, persistently seronegative female sex workers in northern Thailand: Chiang Mai HEPS Working Group. *J. Infect. Dis.* 179: 59–67.
45. Mazzoli, S., D. Trabattoni, S. Lo Caputo, S. Piconi, C. Ble, F. Meacci, S. Ruzzante, A. Salvi, F. Semplici, R. Longhi, et al. 1997. HIV-specific mucosal and cellular immunity in HIV-seronegative partners of HIV-seropositive individuals. *Nat. Med.* 3: 1250–1257.
46. Kaul, R., D. Trabattoni, J. J. Bwayo, D. Arienti, A. Zagliani, F. M. Mwangi, C. Kariuki, E. N. Ngugi, K. S. MacDonald, T. B. Ball, et al. 1999. HIV-1-specific mucosal IgA in a cohort of HIV-1-resistant Kenyan sex workers. *AIDS* 13: 23–29.
47. Barassi, C., A. Lazzarin, and L. Lopalco. 2004. CCR5-specific mucosal IgA in saliva and genital fluids of HIV-exposed seronegative subjects. *Blood* 104: 2205–2206.
48. Dean, M., M. Carrington, C. Winkler, G. A. Huttley, M. W. Smith, R. Allikmets, J. J. Goedert, S. P. Buchbinder, E. Vittinghoff, E. Gomperts, et al. 1996. Genetic restriction of HIV-1 infection and progression to AIDS by a deletion allele of the CKR5 structural gene: Hemophilia Growth and Development Study, Multicenter AIDS Cohort Study, Multicenter Hemophilia Cohort Study, San Francisco City Cohort, ALIVE Study. *Science* 273: 1856–1862.
49. Liu, R., W. A. Paxton, S. Choe, D. Ceradini, S. R. Martin, R. Horuk, M. E. MacDonald, H. Stuhlmann, R. A. Koup, and N. R. Landau. 1996. Homozygous defect in HIV-1 coreceptor accounts for resistance of some multiply-exposed individuals to HIV-1 infection. *Cell* 86: 367–377.
50. Samson, M., F. Libert, B. J. Doranz, J. Rucker, C. Liesnard, C. M. Farber, S. Saragosti, C. Lapoumeroulie, J. Cognaux, C. Forceille, et al. 1996. Resistance to HIV-1 infection in Caucasian individuals bearing mutant alleles of the CCR-5 chemokine receptor gene. *Nature* 382: 722–725.
51. Pastori, C., B. Weiser, C. Barassi, C. Uberti-Foppa, S. Ghezzi, R. Longhi, G. Calori, H. Burger, K. Kemal, G. Poli, et al. 2006. Long-lasting CCR5 internalization by antibodies in a subset of long-term nonprogressors: a possible protective effect against disease progression. *Blood* 107: 4825–4833.
52. Roth-Walter, F., I. Scholl, E. Untersmayr, R. Fuchs, G. Boltz-Nitulescu, A. Weissenbock, O. Scheiner, F. Gabor, and E. Jensen-Jarolim. 2004. M cell targeting with *Aleuria aurantia* lectin as a novel approach for oral allergen immunotherapy. *J. Allergy Clin. Immunol.* 114: 1362–1368.
53. Foster, N., M. A. Clark, M. A. Jepson, and B. H. Hirst. 1998. *Ulex europaeus 1* lectin targets microspheres to mouse Peyer's patch M-cells in vivo. *Vaccine* 16: 536–541.
54. Giannasca, P. J., K. T. Giannasca, A. M. Leichtner, and M. R. Neutra. 1999. Human intestinal M cells display the sialyl Lewis A antigen. *Infect. Immun.* 67: 946–953.
55. Sharma, R., E. J. van Damme, W. J. Peumans, P. Sarsfield, and U. Schumacher. 1996. Lectin binding reveals divergent carbohydrate expression in human and mouse Peyer's patches. *Histochem. Cell Biol.* 105: 459–465.

JVAC95541-7

Vaccine xxx (2009) xxx–xxx

Contents lists available at ScienceDirect

Vaccine

journal homepage: www.elsevier.com/locate/vaccine

T cell-based functional cDNA library screening identified SEC14-like 1a carboxy-terminal domain as a negative regulator of human immunodeficiency virus replication

Emiko Urano [a,b], Reiko Ichikawa [a], Yuko Morikawa [b], Takeshi Yoshida [c], Yoshio Koyanagi [c], Jun Komano [a,*]

[a] National Institute of Infectious Diseases, 1-23-1 Toyama, Shinjuku-ku, Tokyo 162-8640, Japan
[b] Graduate School of Infection Control Sciences, Kitasato University, Shirokane 5-9-1, Minato-ku, Tokyo 108-8641, Japan
[c] Laboratory of Viral Pathogenesis, Institute for Virus Research, Kyoto University, Kyoto 606-8507, Japan

ARTICLE INFO

Article history:
Received 16 May 2009
Received in revised form 7 July 2009
Accepted 24 July 2009
Available online xxx

Keywords:
HIV-1
SEC14L1a
Genome-wide screening

ABSTRACT

Genome-wide screening of host factors that regulate HIV-1 replication has been attempted using numerous experimental approaches. However, there has been limited success using T cell-based cDNA library screening to identify genes that regulate HIV-1 replication. We have established a genetic screening strategy using the human T cell line MT-4 and a replication-competent HIV-1. With this system, we identified the C-terminal domain (CTD) of SEC14-like 1a (SEC14L1a) as a novel inhibitor of HIV-1 replication. Our T cell-based cDNA screening system provides an alternative tool for identifying novel regulators of HIV-1 replication.

1. Introduction

The molecular interaction between HIV-1 and the host is not fully understood. A systematic genome-wide approach provides the critical information for the completion of the HIV-1-host interactome. Many experimental genome-wide screening systems have been established to identify the cellular genes required for HIV-1 replication (Table 1, [1–8]). More than a hundred genes have been identified as being cellular factors that regulate HIV-1 replication. However, different screening systems do not identify the same set of genes, and many systems yielded non-overlapping candidates. These discrepancies are assumed to be due to differences in the experimental approaches, such as the virus, the cell line, or the genetic materials used.

For viruses, the wild-type HIV-1 [1,3–6] or a replication-incompetent HIV-1 pseudotyped with vesicular stomatitis virus (VSV)-G is used [2,7,8]. The VSV-G-pseudotyped "HIV-1-based vector" has been used to identify factors associated with the viral entry processes. However, in reality, it covers the events from post-membrane fusion to translation. One of the potential caveats in the use of the VSV-G-pseudotyped vector is that it enters cells via the VSV-G-restricted route, which is fundamentally different from the HIV-1 *Env*-mediated entry pathway [9–12]. The replication-competent HIV-1 should be ideal to cover the entire viral replication cycle; however, this may raise biosafety concerns.

For cells, non-T cells, such as a genetically engineered HeLa cells that ectopically express luciferase or beta-galactosidase (TZM-bl cells), are often used, since they are efficiently transduced with genetic materials [2,5–8]. Not many studies employ a T cell-based system, partly because genetic materials are not efficiently transduced into T cells [1,3,4]. To identify HIV-1 replication regulatory factors, it is preferable to perform the functional analysis in the natural targets of HIV-1 including T cells. The gene expression profile of non-T cells is apparently different from that of T cells as exemplified by the absence of T cell specific markers on non-T cells such as CD4. It is possible that a candidate gene isolated in the non-T cell-based system might not be expressed in T cells. It is impossible to identify T cell-specific factors in the non-T cell-based screening using the siRNA library or in the screening using cDNA libraries derived from non-T cells. Also, the effect or functions of some genes may not be identical in distinct cell types. The potential risk of a non-T cell-based assay is that we may falsely score a gene as a regulator of HIV-1 replication, although many genes have been discovered using non-T cell-based screening systems including the viral receptors. Ideally, the primary CD4-positive T cells, dendritic cells, macrophages, or NK/T cells should be used.

* Corresponding author at: AIDS Research Center, National Institute of Infectious Diseases, 1-23-1 Toyama, Shinjuku, Tokyo 162-8640, Japan. Tel.: +81 3 5285 1111; fax: +81 3 5285 5037.
E-mail address: ajkomano@nih.go.jp (J. Komano).

0264-410X/$ – see front matter © 2009 Published by Elsevier Ltd.
doi:10.1016/j.vaccine.2009.07.084

Table 1
Summary of genome-wide screening strategies to identify regulatory factors of HIV-1 replication.

Genetic material	Transduction approach	Cell line	Replication competency of HIV-1	Reference
cDNA library	Retroviral, stable	TE671	Incompetent	[2,8]
siRNA library	Transfection, transient	HeLa or 293T	Competent or incompetent	[5,6,7]
cDNA library	Lenti- or retroviral, stable	MT-4	Competent	[1,3,4]

Given technical limitations, this is currently unrealistic for genetic screening experiments.

As for the genetic material, cDNA libraries are often used [1–4,8]. Recent studies utilized siRNA libraries [5–7]. The cDNA approach is advantageous for providing genetic diversity. Expression of the full-length open reading frame of a gene can upregulate the function of the gene, whereas cDNA fragments can function in a diverse fashion. The gene silencing approach downregulates gene expression; however, the silencing efficiency of a gene varies in different cell types and at different time points in the assay (reviewed in [13]). As mentioned above, the gene silencing approach is unable to score the contribution of genes that are not expressed in the cells used in the assay.

The screening can be performed in cells that are either transiently [5–7] or stably [1–4,8] transduced with genetic materials. In the transient transfection assays, it is possible that the dysregulation of a gene function can damage the physiology of the cells. In such a case, the inhibition of HIV-1 replication can be observed, but may not be a direct inhibitory effect of the gene of interest. Such a risk can be minimized by using cells stably transduced with the genetic materials.

We conducted a phenotype cDNA screen using a T cell line-based assay to identify cellular genes that render cells resistant to HIV-1 replication [3]. The advantage of our functional screening system is that cDNA libraries are stably transduced into cells, and that a replication-competent HIV-1 and a human T cell line MT-4 are used. With this system, we have successfully identified the SEC14-like 1a (SEC14L1a) C-terminal domain (CTD) as an inhibitor of HIV-1 replication that targets the late phase of the viral life cycle.

2. Materials and methods

2.1. Cells, transfection, cDNA selection

Cells were maintained in RPMI 1640 medium (Sigma, St. Louis, MA) supplemented with 10% fetal bovine serum (Japan Bioserum, Tokyo, Japan), 100 U/ml penicillin, and 100 μg/ml streptomycin (Invitrogen, Tokyo, Japan). Cells were incubated at 37 °C in a humidified 5% CO_2 atmosphere. Cells were transfected with Lipofectamine 2000 according to the manufacturer's protocol (Invitrogen). The method of selecting human cDNAs that confer resistance to HIV-1 has been described previously in detail [3].

2.2. Plasmids

The SEC14L1a CTD1 was amplified from MT-4 polyA RNA by reverse transcriptase PCR (RT-PCR) using the primers 5'-GCACCGGTCTCGAGCCACCATGGACTACAAAGACGATGACGACCCTGCGTGCGCCGCCAGCAGC-3' and 5'-CCAATTGCTACCTGGAGATCATGGAGCTG-3'. The SEC14L1a CTD2 was amplified by PCR from human lymph node cDNA library (Takara, Otsu, Japan) using the primers 5'-GCACCGGTCTCGAGCCACCATGGACTACAAAGACGATGACGACTGCGAAGTGCCAGAGGGTGGAC-3' and 5'-CCAATTGCTACCTGGAGATCATGGAGCTG-3'. Full length (FL) SEC14L1a was amplified by PCR from a plasmid containing the SEC14L1a open reading frame (ORF, CS0DL004YN18, Invitrogen), using the primers 5'-GCACCGGTCTCGAGCCACCATGGACTACAAAGACGATGACGACGTGCAGAAATACCAGTCCCCAG-3' and 5'-CCAATTGCTACCTGGAGATCATGGAGCTG-3'. The AgeI-MfeI fragments of the PCR products were cloned into the XmaI-MfeI sites of the pEGFP-C3 plasmid (Clontech, Palo Alto, CA), generating pEGFP-SEC14L1a-CTD1, -CTD2, and -FL. The XhoI-MfeI fragments from the resulting plasmids were cloned into the corresponding restriction sites of the pCMMP KRAB vector, creating pCMMP GFP-SEC14L1a-CTD1, -CTD2, and -FL. The HIV-1 *tat* was amplified by PCR using the primers 5'-AACCGGTCTCGAGCCACCATGGAGCCAGTAGATCCTAGAC-3' and 5'-GGATCCTCAGTCGTCATCGTCTTTGTAGTCTTCCTTCGGGCCTGTCGGGTC-3'. A Tat expression vector pCMMP Tat was constructed by cloning the AgeI-BamHI fragment of the PCR product into the corresponding restriction sites of the pCMMP KRAB vector. The HIV-1 *Env* and GFP expression vectors (pIIIex and pCMMP GFP, respectively) are described previously [3,12,14]. To construct the pCMMP GFP-FLAG (GFPf), pCMMP CXCR4 d-10 [15] was digested with AgeI and XhoI to remove CXCR4 d-10 ORF and self-ligated after blunting with T4 DNA polymerase. The HIV-1 *gag-pol*, *tat*, and *rev* expressing plasmid pCMVR8.91 was a generous gift from Dr. Trono's group [16].

2.3. Western blotting

Western blotting was performed according to techniques described previously [17]. The following reagents were used: anti-FLAG (rabbit polyconal, 600-401-383, Rockland, Gilbertsville, PA), anti-p24 (183-H12-5C, NIH AIDS Research and Reference Reagent Program), anti-gp120 (vA-20 and vT-21 antibodies, Santa Cruz Biotech, Santa Cruz, CA), biotinylated anti-goat antibody (GE Healthcare Bio-Sciences, Piscataway, NJ), horseradish peroxidase-conjugated streptoavidin (GE Healthcare Bio-Sciences), and EnVision+ system (Dako, Glostrup, Denmark). Signals were visualized with an LAS3000 imager (Fujifilm, Tokyo, Japan) and quantified by Multi Gauge ver 3.0 software (Fujifilm).

2.4. Confocal microscopy

293T cells transiently transfected with expression vectors for SEC14L1a derivatives were grown on glass plates, fixed in 4% formaldehyde in phosphate buffer saline (PBS) for 5 min at 24 h post-transfection, stained with Hoechst 33258 (Sigma), mounted (Vectorshield, Vector Laboratories, Burlingame, CA), and imaged using a confocal microscope META 510 (Carl Zeiss, Tokyo, Japan). For MT-4 cells, live cells were incubated with Hoechst 33258 and imaged unfixed. Image brightness and contrast were processed by META510 software (Carl Zeiss).

2.5. Immunoprecipitation

Cells expressing FLAG-tagged proteins were harvested and washed twice with PBS and then lysed in the lysis buffer (50 mM Tris–HCl, pH 8.0, 0.5% IGEPAL CA630, protease inhibitor cocktail from Sigma) on ice for 30 min. The soluble fraction was obtained by centrifugation at 15,000 rpm for 30 min at 4 °C, and was incubated with 20 μl of Red-Anti-FLAG M2 Affinity Gel (Sigma) with gentle mixing overnight at 4 °C. After washing the agarose beads for five times with the lysis buffer, the bound complexes were eluted with the FLAG peptide, and analyzed by Western blotting.

Please cite this article in press as: Urano E, et al. T cell-based functional cDNA library screening identified SEC14-like 1a carboxy-terminal domain as a negative regulator of human immunodeficiency virus replication. Vaccine (2009), doi:10.1016/j.vaccine.2009.07.084